PLOS GENETICS

RESEARCH ARTICLE

The CATP-8/P5A-type ATPase functions in multiple pathways during neuronal patterning

Leo T. H. Tang[1☯], Meera Trivedi[2☯], Jenna Freund[2], Christopher J. Salazar[1], Maisha Rahman[2], Nelson J. Ramirez-Suarez[1¤], Garrett Lee[2], Yu Wang[3], Barth D. Grant[3], Hannes E. Bülow[1,2]*

1 Department of Genetics Albert Einstein College of Medicine, Bronx, New York, United States of America, **2** Dominick P. Purpura Department of Neuroscience, Albert Einstein College of Medicine, Bronx, New York, United States of America, **3** Department of Molecular Biology & Biochemistry, Rutgers Center for Lipid Research, Rutgers University, Piscataway, New Jersey, United States of America

☯ These authors contributed equally to this work.
¤ Current address: Institute of Science and Technology Austria, Klosterneuburg, Austria.
* hannes.buelow@einsteinmed.org

Citation: Tang LTH, Trivedi M, Freund J, Salazar CJ, Rahman M, Ramirez-Suarez NJ, et al. (2021) The CATP-8/P5A-type ATPase functions in multiple pathways during neuronal patterning. PLoS Genet 17(7): e1009475. https://doi.org/10.1371/journal.pgen.1009475

Editor: Claire Y. Benard, McGill University, UNITED STATES

Received: March 7, 2021

Accepted: June 10, 2021

Published: July 1, 2021

Data Availability Statement: All relevant data are within the manuscript and its Supporting Information files.

Funding: This work was supported by a fellowship from the Croucher Foundation (https://croucher.org.hk/) to L.T.H.T., A Tishman Scholarship to J.F. (https://einsteinmed.org/departments/neuroscience/), the National Institutes of Health (NIH) R01NS096672 & R21NS111145 (https://www.nih.gov) to H.E.B., R01GM135326, R01GM067237 & R01AG047101 to B.D.G.,

Abstract

The assembly of neuronal circuits involves the migrations of neurons from their place of birth to their final location in the nervous system, as well as the coordinated growth and patterning of axons and dendrites. In screens for genes required for patterning of the nervous system, we identified the *catp-8/P5A-ATPase* as an important regulator of neural patterning. P5A-ATPases are part of the P-type ATPases, a family of proteins known to serve a conserved function as transporters of ions, lipids and polyamines in unicellular eukaryotes, plants, and humans. While the function of many P-type ATPases is relatively well understood, the function of P5A-ATPases in metazoans remained elusive. We show here, that the *Caenorhabditis elegans* ortholog *catp-8/P5A-ATPase* is required for defined aspects of nervous system development. Specifically, the *catp-8/P5A-ATPase* serves functions in shaping the elaborately sculpted dendritic trees of somatosensory PVD neurons. Moreover, *catp-8/P5A-ATPase* is required for axonal guidance and repulsion at the midline, as well as embryonic and postembryonic neuronal migrations. Interestingly, not all axons at the midline require *catp-8/P5A-ATPase*, although the axons run in the same fascicles and navigate the same space. Similarly, not all neuronal migrations require *catp-8/P5A-ATPase*. A CATP-8/P5A-ATPase reporter is localized to the ER in most, if not all, tissues and *catp-8/P5A-ATPase* can function both cell-autonomously and non-autonomously to regulate neuronal development. Genetic analyses establish that *catp-8/P5A-ATPase* can function in multiple pathways, including the Menorin pathway, previously shown to control dendritic patterning in PVD, and Wnt signaling, which functions to control neuronal migrations. Lastly, we show that *catp-8/P5A-ATPase* is required for localizing select transmembrane proteins necessary for dendrite morphogenesis. Collectively, our studies suggest that *catp-8/P5A-ATPase* serves diverse, yet specific, roles in different genetic pathways and may be involved in the regulation or localization of transmembrane and secreted proteins to specific subcellular compartments.

F31NS111939 to M.T., F31NS100370 to M.R., T32GM007491 to C.J.S., P40 OD010440, and to Caenorhabditis Genetics Center at the University of Minnesota, P30CA013330 & P30HD071593 to Albert Einstein College of Medicine. The funders had no role in study design, data collection and analysis, decision to publish, or preparation of the manuscript. The authors have not financial conflicts of interest to declare.

Competing interests: The authors have declared that no competing interests exist.

Author summary

P-type ATPases are a large family of transporters that are conserved from unicellular eukaryotes and plants to metazoans. Structurally and functionally, they fall into five subfamilies, P1 to P5, of which the latter is further divided into P5A and P5B-type ATPases. Unlike for other P-type ATPases, no mutant phenotypes for the P5A-type ATPases have been described in metazoans. Here, we show that the *catp-8/P5A-ATPase* in the nematode *Caenorhabditis elegans* is involved in multiple aspects of neuronal patterning, including neuronal migrations as well as axon guidance and dendrite patterning. A functional fluorescent reporter fusion shows the CATP-8/P5A-ATPase is expressed in most, if not all, tissues in the endoplasmic reticulum and that *catp-8* can function both in neurons and surrounding tissues from where it orchestrates neuronal development. Genetically, *catp-8* acts in multiple pathways during these processes, including the Wnt signaling and the Menorin pathway. Imaging studies suggest that the *catp-8/P5A-ATPase* is necessary for proper localization of cell-surface transmembrane proteins to dendrites of sensory neurons, but likely not for their trafficking. In summary, we propose that CATP-8/P5A-ATPase serves a function in the ER during development of select neurons, by localizing certain transmembrane, and possibly, secreted proteins.

Introduction

Development of a nervous system is a crucial step in metazoan development that requires the coordinated interactions of many genetic pathways and tissues. This process can be broken down into at least three components. First, in metazoans, a majority of neurons are actually born distant from their final location in adult animals. Therefore, neurons have to migrate from the place where they are born to their final location in the nervous system, a process that is guided by both intrinsic and extrinsic factors [1,2]. Second, axonal processes, the cellular structures that mediate output of nerve cells, need to grow and navigate, guided by extracellular guidance factors, towards their cellular targets with whom they form specific synaptic connections [3,4]. Third, the often elaborately sculpted dendrites, a neuron's receiving cellular structures, are patterned by dedicated pathways that originate from different tissues and act both cell-autonomously and non-autonomously [5–7].

The nematode is an excellent system to study basic aspects of conserved processes involved in neural patterning. Several cellular paradigms in worms can be studied at single cell resolution, and often, ample genetic information already exists for these processes. For example, the somatosensory PVD neurons are a powerful system to study conserved mechanisms of dendrite patterning [8,9]. These mechanisms involve the interactions of different tissues that coordinately establish the stereotyped dendritic trees of PVD neurons. A complex of two transmembrane cell adhesion molecules, SAX-7/L1CAM and MNR-1/Menorin, function from the skin in concert with a secreted chemokine LECT-2/Chondromodulin II from muscle to instruct the growing PVD dendrites via a leucine rich transmembrane receptor DMA-1/LRR-TM expressed in dendrites [8,9]. Other well-studied paradigms include neuronal migrations, such as the anteriorly directed embryonic migration of hermaphrodite specific (HSN) neurons from the tail region towards the midbody region [10] or the pair of laterally located Q neuroblasts, which undergo stereotypical divisions and migrations during larval stages [11]. All cell migrations appear to be controlled, at least in part, by the conserved Wnt signaling system, among others [12,13].

The diverse P-type ATPase family of transporters is an evolutionarily highly conserved family of transporters in eukaryotes that, respectively, move multiple molecular species, including ions and lipids across membranes through the hydrolysis of ATP. These P-type ATPases are multi-transmembrane proteins that can be divided into five subfamilies based on structural and functional characteristics, P1 through P5 [14,15], of which the latter can be further divided into the P5A and P5B family [16]. The P1 through P3 subfamilies serve as ion transporters, whereas the P4 subfamily has been shown to function as flippases that move lipids across membranes [15]. The P5B family of transporters was recently reported to transport polyamines across membranes [17]. Mutations in the P5A family of transporters in both plants (*A. thaliana*) and unicellular eukaryotes (*S. cerevisiae*) were shown to display pleiotropic phenotypes, including defects in phosphate homeostasis and male gametogenesis [18–20], phospholipid and sterol homeostasis [21], and targeting of mitochondrial outer membrane proteins [22]. However, it remained unclear what functions P5A-ATPases serve in metazoans.

We show here that the sole *C. elegans* ortholog *catp-8/P5A-ATPase* is required for specific aspects of nervous system development, including dendrite patterning, axonal guidance decisions and neuronal migrations. A CATP-8/P5A-ATPase reporter shows expression in the endoplasmic reticulum in most if not all tissues albeit at different levels. Moreover, the *catp-8/P5A-ATPase* can function both cell-autonomously and non-autonomously in multiple genetic pathways in to regulate neuronal development. Additionally, we find that in *catp-8/ATPase* mutants, the amounts of functional reporters for select transmembrane proteins (the leucine rich transmembrane receptor DMA-1/LRR-TM and the HPO-30/Claudin-like molecule) are strongly reduced on higher order dendritic branches of PVD dendrites. Taken together, these results suggest that the CATP-8/P5A-ATPase functions in multiple pathways during neural patterning and is important for correct localization of transmembrane cell surface proteins and possibly secreted proteins. While this study was in progress, two studies reporting a function for *catp-8/P5A-ATPase* in PVD patterning in *C. elegans* were published [23,24]. Feng et al. suggested a role for *catp-8/P5A-ATPase* in dendrite patterning and targeting of DMA-1/LRR-TM in dendrites [23] and Qin et al. suggested that *catp-8* was important for ER homeostasis by preventing mistargeting of mitochondrial proteins independently of ER-associated degradation (ERAD) as well as dendrite patterning [24]. Similarly, a crystal structure of the yeast homolog Spf1 in conjunction with biochemical studies suggested a role for P5A-ATPases in ER and mitochondrial quality control [25].

Results

The P5A-type ATPase CATP-8 is required for somatosensory dendrite patterning

In a genetic screen for animals with defects in dendrite arborization of PVD somatosensory neurons, we isolated the allele *dz224* with characteristic defects in dendrite patterning of PVD. Using a combination of whole genome sequencing and mapping (S1 Fig, Materials and Methods)[26]), we found that the molecular lesion in *dz224* results in a premature stop codon after 55 amino acids in *catp-8*, which encodes the sole P5A-type ATPase in the *C. elegans* genome (Fig 1A–1C). Based on the molecular nature of *dz224*, we predict this allele to result in strong, if not complete loss of function of the *catp-8/P5A-ATPase*.

To more precisely determine the function of *catp-8* in dendrite patterning, we conducted morphometric analyses of PVD somatosensory dendrites. During larval stages two primary dendrites emanate from the PVD cell body on either side of the animal in an anterior and posterior direction, respectively, and through sequential perpendicular branching of secondary, tertiary, and quaternary branches establish highly stereotyped dendritic trees with semblance

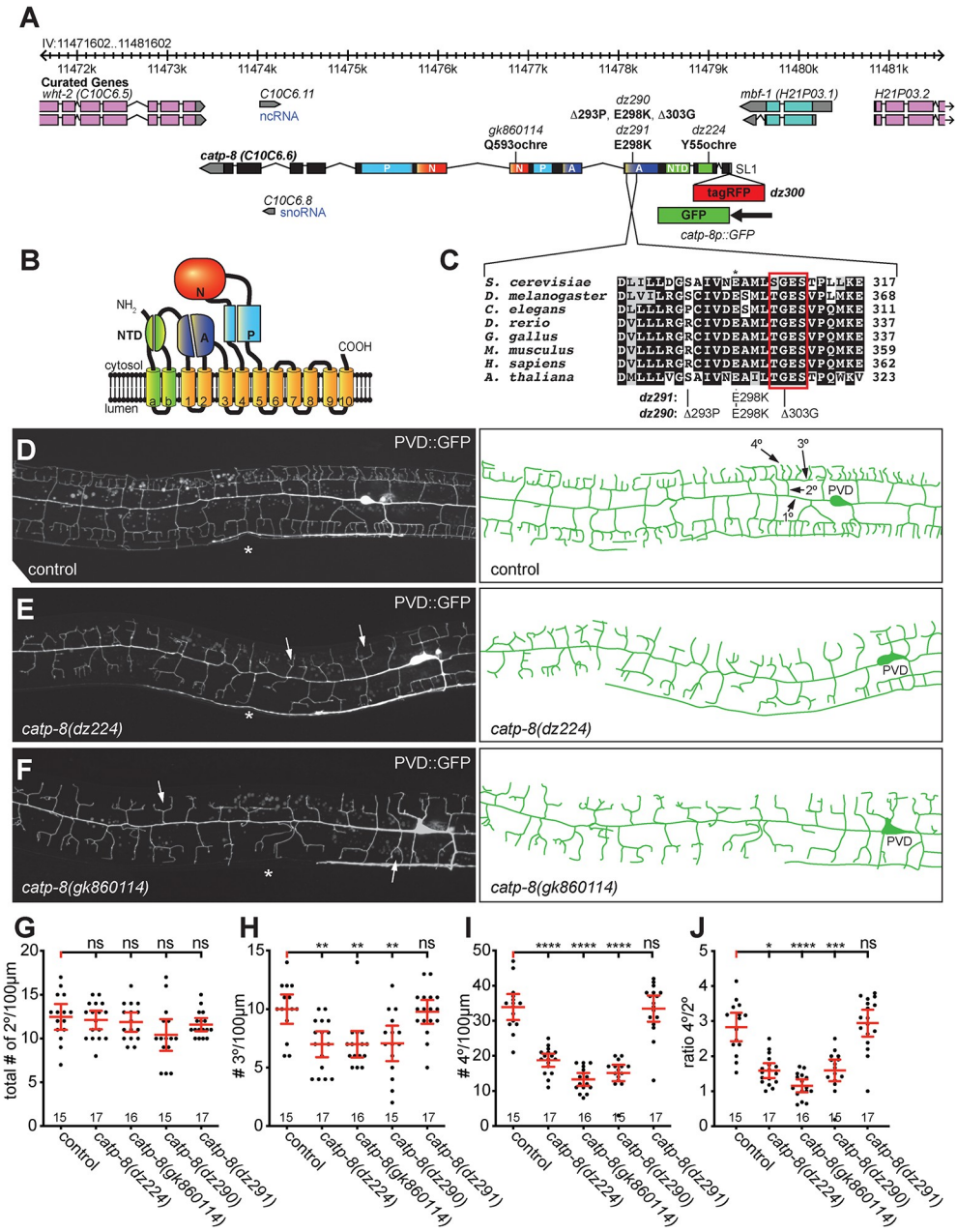

Fig 1. CATP-8/P5A-ATPase is required for PVD dendrite patterning. A. Genetic environs of the *catp-8* locus on chromosome IV. *catp-8* is encoded on the minus strand and transcribed from right to left. Alleles used in this study are indicated as are the resulting molecular changes. The *catp-8* transcript can be SL1 spliced based on the *yk1435b05* EST clone (gift of Y. Kohara). Since *catp-8* has also been suggested to be SL2 spliced [23], *catp-8* may be part of a hybrid operon. Parts of the exons that encode specific domains are color coded and designated as: NTD: N-terminal domain, A: actuator domain, N: nucleotide binding domain, P: phosphorylation domain. A schematic of the *catp-8p*::*GFP* transcriptional reporter is shown as is the genomic location of the tagRFP insertion to create the translational tagRFP::CATP-8 reporter. B. Schematic domain structure and membrane topology of the CATP-8/P5A ATPase with the domains labeled and color coded as in A. C. Alignment of a conserved section of the actuator domain encoding a phosphatase activity, which is required for functional cycling of P-type ATPases [15]. The E298K mutation (asterisk, equivalent to the E349K mutant associated with intellectual disability [32]) is immediately adjacent to the (S/T)GES loop (boxed in red), which is important for A-domain function [25]. Noted on the right is the number of amino acids. Accession numbers of sequences for P5A-type ATPases used in the alignment are P39986 (*S. cerevisiae*), Q9VKJ6 (*D. melanogaster*), P90747 (*C. elegans*), F1R1X4 (*D. rerio*), Q5ZKB7 (*G. gallus*), Q9EPE9 (*M. musculus*), Q9VKJ6 (*H. sapiens*), Q9LT02 (*A. thaliana*). D. -F. Fluorescent micrographs of PVD neurons with corresponding schematics on the right in the genotypes indicated. PVD was visualized with *wdIs52* (*Is[F49H12.4p*::*GFP]*) [28]. Asterisks mark the

location of the vulva. In D., primary (1˚), secondary (2˚), tertiary (3˚) and, quaternary (4˚) dendrites are indicated. White arrows in E. and F. indicate typical *catp-8* mutant defects. G.—J. Quantification of the number of secondary (G), tertiary (H), and quaternary (I) dendrite branches, as well as the ratio of quaternary to secondary (J) branches, 100 μm anterior to the PVD cell body in the genotypes indicated. Data are represented as the mean ± 95% confidence interval. Statistical significance was calculated using one-sided ANOVA with Tukey's multiple comparison test. * $P \leq 0.05$, ** $P \leq 0.01$, *** $P \leq 0.001$, **** $P \leq 0.0001$, ns not significant. n = 15 wild-type control (*wdIs52*) animals; n = 17 *catp-8 (dz224)* mutant animals; n = 16 *catp-8(gk860114)*; n = 15 *catp-8(dz290)*; n = 17 *catp-8(dz291)*.

https://doi.org/10.1371/journal.pgen.1009475.g001

to Menorah-like candelabras (Fig 1D)[27–29]. We traced dendrites in a region 100μm anterior to the cell body of young adult animals and determined the number and length of secondary, tertiary and quaternary dendritic branches. Compared to wild type animals, we found the total number of secondary branches unchanged, whereas the number of tertiary and quaternary branches were significantly reduced in *catp-8(dz224)* mutants (Fig 1E and 1G–1I). However, the number of secondary branches that reached the line of the tertiary branches was significantly reduced, resulting in a reduced aggregate length of secondary branches (S1B and S1C Fig). Overall, many dendritic trees displayed a conspicuous defect, where secondary branches appeared to lack proper tertiary branches, and merely bifurcated into two quaternary dendrites rather than forming perpendicular tertiary branches. This observation was also borne out by a reduced number of quaternary branches per secondary branches, approaching an average of two quaternary branches per secondary branch (i.e. per menorah) as opposed to approximately four in control animals, and a decrease in aggregate length of secondary, tertiary and quaternary branches (Figs 1J and S1B–S1E). In addition, we observed increased numbers of ectopic secondary and ectopic tertiary branches, possibly reflective of a lack of a functioning feed-back loop that has been postulated to restrict secondary branching once stable tertiary branches have been formed [30].

To corroborate these findings, we obtained three additional alleles of *catp-8/P5A ATPase*, including *gk860114* from the million mutation project [31], which results in a premature stop codon after 593 amino acids (Fig 1A). We used CRISPR/Cas9 based genome editing to create two additional alleles (Fig 1A and 1C): *dz290*, which deletes two codons within a perfectly conserved stretch of the actuator domain [15], and a missense mutation (E289K), which changes a perfectly conserved glutamic acid to lysine (E289K) in the actuator domain (Fig 1A and 1C), and is analogous to a mutation described in a pair of sisters with intellectual disability [32]. Finally, we introduced the E289K mutation on its own to create *dz291*. Of these, all but the *dz291* allele displayed strong phenotypes in PVD patterning that were indistinguishable from the *dz224* allele (Figs 1G–1J and S1B–S1E). Consistent with the nonsense mutations in *dz224* and *gk860114*, both alleles behaved recessively and failed to complement each other, suggesting loss of *catp-8* function (S1F Fig). To test, whether the *gk860114* allele behaved genetically as a null allele, we analyzed animals where *catp-8(gk860114)* was placed in trans to the *mDf7* deficiency, which removes the genomic region encoding *catp-8* and fails to complement *catp-8* mutant alleles (S1A Fig). We found that these animals did not display a more severe phenotype in PVD patterning than *catp-8(gk860114)* homozygous animals, demonstrating that *gk860114* behaves as a genetic null allele (S1G Fig). Animals carrying the *catp-8(gk860114)* null allele appear superficially normal, have a normal body length at the L1 larval stage (S1H Fig), but seem to grow slower. Taken together these findings suggest that *catp-8* function is required for PVD patterning, especially for the extension of tertiary and quaternary dendritic branches. Moreover, the E289K mutation, which is analogous to a mutation shared by the pair of sisters with intellectual disability [32], does not compromise *catp-8* sufficiently to result in morphological phenotypes, at least in the context of PVD patterning or neuronal migration (see below). Lastly, the defects due to mutations in the actuator domain are consistent with the

interpretation that enzymatic activity of CATP-8/P5A type ATPase is required for PVD patterning.

The P5A-type ATPase CATP-8 is required for specific neuronal and axonal migrations

We next asked whether *catp-8* is only necessary for development of the highly branched dendritic trees of PVD dendrites or more generally, for other aspects of neural patterning. To this end, we crossed *catp-8* mutants with a panel of GFP reporters that label individual neurons or classes of neurons, including motor neurons, interneurons, sensory neurons and touch receptor neurons. We found that mutant alleles of *catp-8* displayed defects in neurite patterning of some but not all neurons. For example, in *catp-8* mutant animals the D-type motor neurons displayed neurite extension defects in the ventral and dorsal nerve cords, whereas the DA/DB-motor neurons appeared indistinguishable from control animals (Table 1, S2A–S2D Fig). This is significant insofar as the processes of both types of motor neurons make similar navigational choices and travel, at least in the nerve cords, in the same fascicles. However, neither patterning of the pair of AIY interneurons, nor the amphid sensory neurons or phasmid sensory neurons was obviously dependent on *catp-8* function (Table 1, S2E–S2J Fig). Lastly, we investigated axon guidance choices of HSN and PVQ neurons at the ventral midline, where both neurons send axons in the left and right ventral nerve cords from the midbody or tail to the head region, respectively. We observed significant defects in axon midline guidance of HSN neurons with cross overs, but no defects for PVQ neurons (Table 1, S2K–S2N Fig). Taken together, our findings show that axonal patterning of some but not all neurons is dependent on *catp-8/P5A-ATPase* function. Importantly, even neurons that make similar guidance choices and travel in the same nerve fascicles such as the D-type and DA/DB motor neurons or the HSN and PVQ neurons, can develop either dependent on *catp-8* function or, independently.

We next investigated a set of stereotyped neuronal and non-neuronal cellular migrations, including both embryonic and postembryonic migrations, as well as anteriorly-posteriorly and posteriorly-anteriorly directed migrations (Fig 2A). We first investigated two embryonic migrations: the pair of ALM mechanosensory neurons, which migrate from the head region towards the midbody region (i.e. anteriorly-posteriorly directed), and the hermaphrodite specific neurons (HSNs), a set of motor neurons that migrate from the tail towards the mid body region (i.e. posteriorly-anteriorly directed)[33]. Loss of *catp-8* function resulted in severe migration defects in anteriorly directed HSN migrations, which often failed to reach their final destination around the midbody and instead stopped migration prematurely (Fig 2B and 2E). In contrast, loss of *catp-8* had no effect on posteriorly directed ALM neuronal migrations (Fig 2C and 2F). We next investigated a set of postembryonic migrations, specifically of the Q cell descendants [11]. The bilateral pair of Q cells are neuroblast cells, which are born during the mid L1 larval stage. On the right side of the animal, the QR cell migrates anteriorly while undergoing a series of stereotyped cell divisions as follows. The first division results in two more blast cells, of which one divides again and gives rise to the AQR cell and the other undergoes programmed cell death [34]. The other blast cell also gives rise to one cell that undergoes programmed cell death and another that after a further division forms the AVM and SDQR neurons (Fig 2A). The AQR and AVM/SDQR neurons therefore originate from two subbranches of QR cell descendants, and are positioned in the head or a lateral anterior section of the worms, respectively. The Q cell descendants on the left side of the animal undergo a posteriorly directed migration while also giving rise, in a similar pattern of divisions, to PQR and PVM/SDQL neurons (Fig 2A). PQR travels to the tail whereas PVM and SDQL remain in a

Table 1. Survey of neuroanatomical defects in *catp-8/P5A-ATPase* mutant animals.

Neurons Examined (Marker Used)	control [%]	*N*	*catp-8* [%]	*N*	*P Value*[1]
Motor Neurons[2]					
D-Type (*juIs76*)					
Gaps in ventral nerve cord	10.8	93	41.3	109	****
Gaps in dorsal nerve cord	12.9	93	26.6	109	*
0 L/R choice commissure	60.0	40	23.6	55	***
1 L/R choice commissure	25.0	40	41.8	55	**
≥ 2 L/R choice commissure	15.0	40	32.7	55	
defasciculation of DNC	0.0	31	11.4	44	0.07
defasciculation of VNC	19.4	31	36.4	44	0.13
defasciculation in both	3.2	31	2.3	44	ns
DA/DB (*evIs82b*)					
Gaps in ventral nerve cord	0	102	0	108	ns
Gaps in dorsal nerve cord	0	102	0	108	ns
L/R choice of commissures	4.8	102	5.7	108	ns
HSN (*mgIs71*)					
Ventral nerve cord crossover[2]	0.0	85	12.5	72	***
Interneurons[3]					
PVQ (*oyIs14*)					
Ventral cord crossover	11.8	101	7	100	ns
AIY (*mgIs32*)					
Early termination	0	120	0	124	ns
Ectopic axonal branching	2	120	2	124	ns
Amphid Neurons[4]					
DiI Stain					
Defasciculation	6	50	4	50	ns
Early termination	0	50	0	50	ns
Anterior process	0	50	0	50	ns
Anterior nerve ring	0	50	0	50	ns
Posterior process	0	50	0	50	ns
Posterior nerve ring	0	50	0	50	ns
Phasmid Neurons[3]					
DiI Stain					
Ectopic axons	0	50	0	50	ns
Axon crossover	0	50	0	50	ns
Wandering processes	0	50	0	50	ns

[1] Statistical significance was calculated using Fisher's exact test.

*, $P \leq 0.05$

**, $P \leq 0.005$

****, $P \leq 0.0001$; ns, not significant.

[2] Note that the cross over defects invariably occurred when HSNL failed to migrate, in which case a process first grew out posteriorly, before turning ventrally. The process then crossed the midline and grew anteriorly in the right ventral nerve cord.

[3] Neuroanatomical defects were scored as described [65].

[4] Neuro-anatomical defects were scored as described [66].

https://doi.org/10.1371/journal.pgen.1009475.t001

lateral posterior section of the animals. We found that the anteriorly directed migrations of both AQR and AVM, which represent both sub branches of QR descendants, are not obviously affected in *catp-8* mutants, whereas the posteriorly directed migrations of PQR and PVM

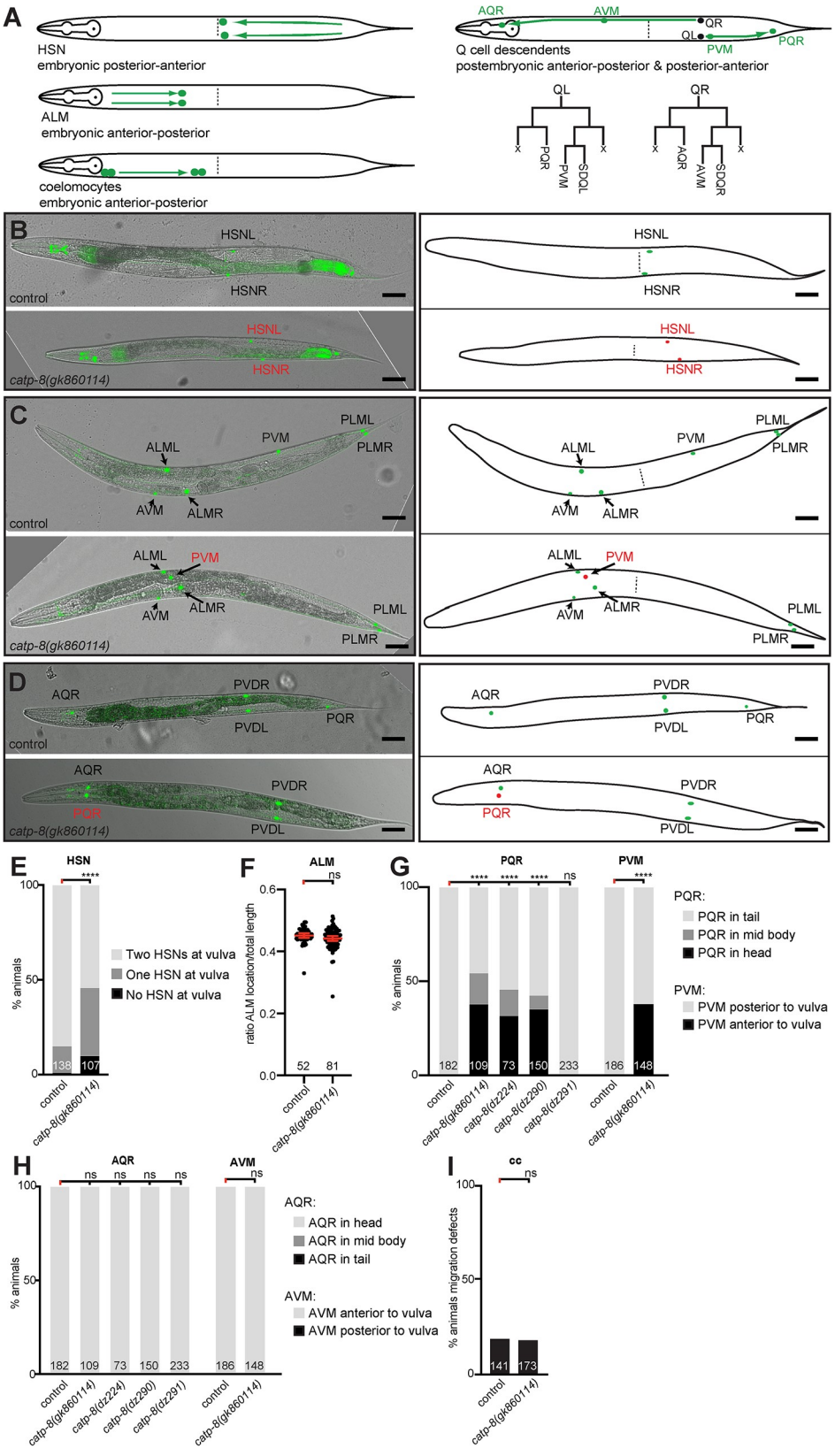
A
HSN
embryonic posterior-anterior
ALM
embryonic anterior-posterior
coelomocytes
embryonic anterior-posterior
AQR
AVM
QR
QL
PQR
PVM
Q cell descendents
postembryonic anterior-posterior & posterior-anterior
QL
QR
PQR
PVM
SDQL
AQR
AVM
SDQR
B
HSNL
HSNR
control
catp-8(gk860114)
C
PLML
ALML
PVM
PLMR
AVM
ALMR
control
catp-8(gk860114)
D
AQR
PVDR
PVDL
PQR
control
catp-8(gk860114)
E
HSN
% animals
Two HSNs at vulva
One HSN at vulva
No HSN at vulva
138
107
F
ALM
ratio ALM location/total length
52
81
G
PQR
PVM
PQR:
PQR in tail
PQR in mid body
PQR in head
PVM:
PVM posterior to vulva
PVM anterior to vulva
182
109
73
150
233
186
148
control
catp-8(gk860114)
catp-8(dz224)
catp-8(dz290)
catp-8(dz291)
H
AQR
AVM
AQR:
AQR in head
AQR in mid body
AQR in tail
AVM:
AVM anterior to vulva
AVM posterior to vulva
I
cc
% animals migration defects
141
173

Fig 2. CATP-8/P5A-ATPase is required for neuronal migrations. A. Schematics of different cellular migrations. Shown on the left are embryonic migrations including HSN (posterior to anterior), ALM (anterior to posterior) and coelomocytes (anterior to posterior). For simplicity, all migrations are illustrated in adult animals. Indicated on the right are the migrations of the descendants of the QL and QR neuroblasts, respectively, which arise in stereotyped cell-divisions as indicated below. Note that Q cells divide into distinct sub-branches, comprising the AQR/PQR or AVM/PVM and SDQR/SDQL neurons, respectively. X denotes cells that undergo programmed cell death [34]. B.—D. Composite of fluorescent and differential interference contrast images of reporters visualizing the HSN neurons (B), touch receptor neurons (C) or AQR/PQR (D). Images of wild type and *catp-8(gk860114)* mutant animals are shown in top and lower panels, respectively, with corresponding schematics on the right. Correctly positioned neurons are shown in green and incorrectly positioned neurons in red. HSN visualized by *dzIs75 II Is[kal-1p9::GFP; ttx-3p::mCherry]*[47]), AQR/PQR by *wdIs52 II Is[F49H12.4p::GFP]*, and touch receptor neurons by *zdIs5 I Is[mec-4p::GFP]* [67]. Scale bar = 25μm. E. Quantification of cell migration defects of HSN neurons. Percent animals are shown with neurons in wild type position (light grey bars), partially incomplete migration (dark grey bars) and completely failed migration (black bars). Pairwise statistical significance was calculated using Fisher's exact test. **** $P \leq 0.0001$, ns not significant. F. Quantification of ALM migration by comparing the ratio of ALM distance from the tip of the nose to the total animal length in control versus *catp-8(gk860114)* mutant animals. Unpaired t test, ns, not significant. G.—H. Quantification of migration of PQR and PVM (G) and AQR and AVM (H) neurons comparing control versus indicated alleles of *catp-8*. Percent animals are shown with neurons in wild type position (light grey bars), partially incomplete migration (dark grey bars) and completely failed migration (black bars). Pairwise statistical significance was calculated using Chi-squared test or Fisher exact test. **** $P \leq 0.0001$; ns, not significant. I. Percentage of animals exhibiting coelomocyte migratory defect in wildtype or *catp-8(gk860114)* mutant animals. Fisher's exact test. ns not significant.

https://doi.org/10.1371/journal.pgen.1009475.g002

neurons display defects (Fig 2C, 2D, 2G, and 2H). Specifically, PQR and PVM erroneously migrate anteriorly towards the head instead of posteriorly. This observation suggests that the choice of directionality in migration of QL descendants on the left side of the animals is dependent on *catp-8/P5A ATPase* function, rather than migratory capacity itself. Moreover, we found that *gk860114* homozygous mutants originating from homozygous mothers displayed Q cell migration defects, whereas *gk860114* homozygous mutants originating from *gk860114/+* heterozygous animals did not display this phenotype, suggesting a maternal contribution of *catp-8* during this postembryonic migration (S1I Fig). In contrast, we observed a similar range of defects in HSN migration and PVD dendrite patterning in *gk860114* homozygous mutants coming from heterozygous mothers compared to those originating from homozygous mothers (S1F and S1J Fig, cf also Fig 2E), leading us to conclude that Q cell migration requires less *catp-8* function compared to HSN and PVD patterning. Lastly, we investigated two pairs of non-neuronal cells, the coelomocytes, which migrate embryonically in a posterior direction [33]. We found that coelomocyte migration proceeds normally in *catp-8* mutants (Fig 2I). Collectively, our experiments show that both embryonic and postembryonic cell migrations require *catp-8/P5A-ATPase* function, including anteriorly and posteriorly directed migrations.

CATP-8/P5A ATPase functions both cell-autonomously and non-autonomously in neural patterning

To gain insight into the cellular focus of action of the *catp-8/P5A-ATPase*, we used CRISPR/Cas9 engineering to insert a tagRFP fluorescent protein at the N-terminus of CATP-8 (Fig 1A). We found these animals to show widespread, if not ubiquitous expression of CATP-8, including in the epidermis, muscle, pharynx, intestine, and the major neuronal ganglia (Fig 3A–3D). The expression appears intracellular in a perinuclear pattern and different tissues appear to express different levels of CATP-8. Of note, we detected expression in both neurons that were phenotypically affected in *catp-8* mutants as well as neurons that were not visibly affected. For example, clear expression of the endogenous tagRFP::CATP-8 reporter was seen in HSN, PVM, and PVD neurons, but also in ALM neurons and others (Fig 3E–3H). Importantly, PVD morphology and PQR cell position appeared completely normal in animals carrying the endogenous fluorescent tag, suggesting that the N-terminal tagRFP::CATP-8 fusion is

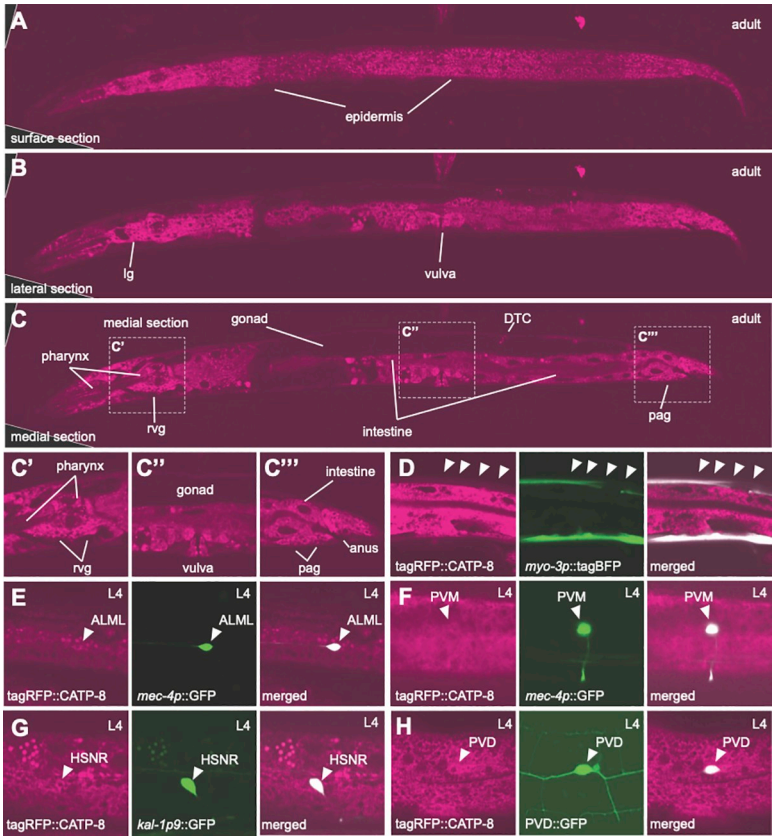

Fig 3. CATP-8/P5A-ATPase is widely expressed at apparently different levels. A.- C. Whole body confocal optical sections of tagRFP translational knock-in of *catp-8* animals, showing perinuclear expression in the tissues indicated. An optical section near the surface of the animals shows epidermal expression, whereas a more lateral and a medial section reveal many other tissues, including pharynx, intestine, lateral ganglion (lg), retrovesicular ganglion (rvg), distal tip cell (DTC), and preanal ganglion (pag). Insets in C are shown magnified as C', C", C"'. Note that tagRFP::CATP-8 is not visibly expressed in the gonad and that expression levels vary in different tissues (e.g. compare epidermal and muscle expression, confer with D). D.- H. Confocal images showing CATP-8 expression in indicated neurons and tissues, as shown by colocalization of tagRFP::CATP-8 with relevant markers, including *dzEx2136* (*Ex[myo-3p::tagBFP; mec-4p::catp-8]* for muscle, D), *zdIs5* (*Is[mec-4p::GFP]* for ALM and PVM, E, F), *dzIs75* (*Is[kal-1p9::GFP]* for HSN, G), *wdIs52* (*Is[F49H12.4p::GFP]* for PVD, H).

https://doi.org/10.1371/journal.pgen.1009475.g003

fully functional. We found similar expression patterns in transgenic animals expressing GFP under control of the *catp-8* 5' region immediately upstream of the ATG start codon, where we also saw widespread expression from embryonic stages onwards, including in muscle, intestine, pharynx and other tissues (S3 Fig). Collectively, our studies show that *catp-8* is widely, if not ubiquitously, expressed albeit at different levels.

A functional CATP-8/P5A ATPase fusion localizes to the endoplasmic reticulum

Previous work showed that the yeast Spf1 (and Arabidopsis MALE GAMETOGENESIS IMPAIRED ANTHERS (MIA) or PDR2) homologs are localized to the endoplasmic reticulum (ER)[19,20,35]. We therefore aimed to determine the subcellular localization of CATP-8 in *C. elegans*. To this end, we used the functional N-terminal fusion of tagRFP to CATP-8 and drove expression from a single copy insertion transgene under control of the heterologous *dpy-7p* promoter, which is specific for the epidermis [36]. We chose to use this single copy, functional

transgene over the endogenously tagged *catp-8* locus to minimize interference with signal from other tissues (cf. Fig 3). This epidermally-expressed transgene (*dzSi3*), which also displayed perinuclear staining (and rescued PVD patterning defects) was crossed with a panel of organellar reporters—for (1) the ER, (2) the cis/medial Golgi, (3) early endosomes, (4) late endosomes and lysosomes, (5) autophagosomes, and (6) lysosomes. We found the strongest colocalization with a marker for the ER and no correlation with markers for Golgi, late endosomes or lysosomes (Fig 4). These findings suggest that in metazoans CATP-8/P5A-ATPase is localized to the ER similarly to plants and unicellular eukaryotes. We next tested whether the gross morphology of these cellular compartments was defective in *catp-8* mutant animals. We found no apparent defects in the perinuclear localization, patterns or intensity of any of the organelle reporters examined (S4 Fig). Taken together, our findings suggest that the CATP-8/P5A-ATPase serves a function in the ER, which may be conserved from unicellular eukaryotes and plants to animals.

CATP-8/P5A ATPase can serve both cell-autonomous and cell-non-autonomous functions during neural patterning

To determine where *catp-8* may function during different developmental processes, we performed transgenic rescue experiments, where we expressed a *catp-8* cDNA under control of heterologous promoters in *catp-8* mutant animals. We found that patterning defects of PVD dendrites were rescued by pan-neuronal transgenic expression of *catp-8*, but not by expression in muscle (Figs 5A–5G and S5A–S5C). Interestingly, a single copy transgene expressing the functional N-terminal tagRFP::CATP-8 fusion under control of the heterologous epidermis-specific *dpy-7p* promoter also rescued PVD patterning defects in *catp-8* mutants (Figs 5A–5G and S5A–S5C). These observations suggest that *catp-8* can serve redundant functions in different tissues, i.e. both cell-autonomously and non-autonomously, but may be sufficient in either neurons or the epidermis. Surprisingly, embryonic and postembryonic cell migration defects of HSN, PQR and, PVM neurons were completely rescued by expression of *catp-8* in muscle, but not in the epidermis, the touch receptor neurons (i.e. PVM), or the precursors that give rise to the Q cells (Figs 5H–5J and S5D and S5E). One out of three transgenic lines expressing the *catp-8* cDNA under control of a pan-neuronal reporter showed partial rescue of the neuronal migration defects of PVM and PQR neurons (Figs 5I,5J and S5D and S5E), suggesting that overexpression in neurons can partially compensate for loss of *catp-8* in other tissues, e.g. muscle. We conclude that at least for these cellular migrations, *catp-8* appears to function non-autonomously in muscle. Therefore *catp-8* can serve both autonomous and non-autonomous functions during neural patterning, including in dendrite morphogenesis and different neuronal migrations.

CATP-8/P5A ATPase functions in the Menorin pathway to pattern PVD dendrites

The conserved Menorin pathway shapes somatosensory patterning of PVD dendrites [8,9]. Briefly, the two putative cell adhesion molecules SAX-7/L1CAM and MNR-1/Menorin form a complex in the epidermis, which, together with the muscle derived chemokine LECT-2/Chondromodulin II forms a high affinity substrate for the leucine rich repeat transmembrane receptor DMA-1/LRR-TM, which functions in PVD neurons [8,9]. Downstream of DMA-1/LRR-TM in PVD, a conserved set of intracellular molecules such as the TIAM-1/GEF guanine nucleotide exchange factor and HPO-30/Claudin act together to regulate the actin cytoskeleton [8,9,37]. Previous genetic experiments established that SAX-7/L1CAM, LECT-2/Chondromodulin II and MNR-1/Menorin function in a linear genetic pathway with the DMA-1/

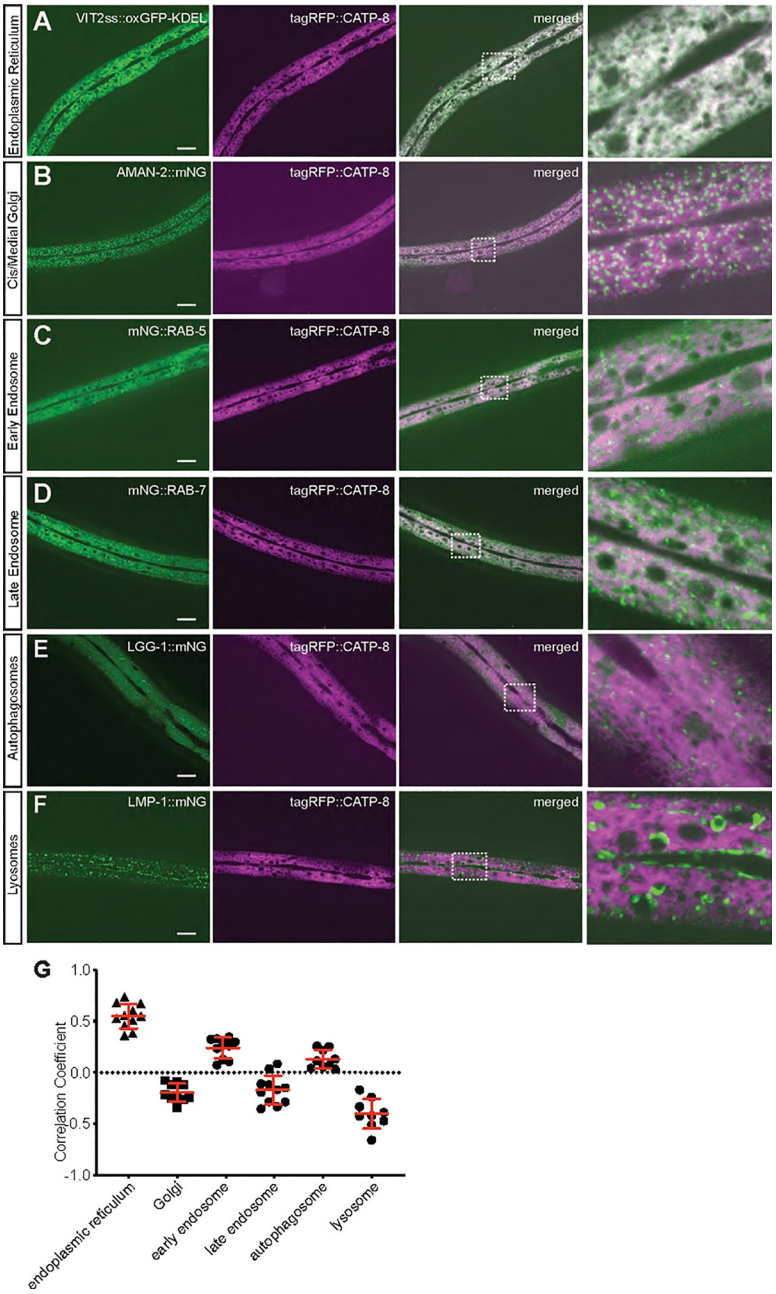

Fig 4. CATP-8/P5A-ATPase localizes primarily to the endoplasmic reticulum. A.—F. Confocal images of animals expressing a functional *tagRFP::CATP-8* fusion under control of the epidermal specific promoter *dpy-7p* from a single copy transgene, in combination with single copy organellar markers for the endoplasmic reticulum (A, *pwSi82[Phyp-7::VIT2ss::oxGFP-KDEL]*), cis/medial Golgi (B, *pwSi202[Phyp7::AMAN-2::mNG;HYG-R]*), early endosomes (C, *pwSi145[Phyp7::mNG::RAB-5;HYG-R]*), late endosomes and lysosomes (D, *pwSi140[Phyp7::mNG::RAB-7;HYG-R]*), autophagosomes (E, *pwSi144[Phyp7::mNG::LGG-1;HYG-R]*), and lysosomes (F, *pwSi205[Phyp7::LMP-1::mNG; HYG-R]*). The right column represents magnifications of the insets indicated. G. Co-localization quantification between tagRFP::CATP-8 and respective cellular compartment markers.

https://doi.org/10.1371/journal.pgen.1009475.g004

LRR-TM receptor, but also suggested that DMA-1 can serve functions in PVD patterning that are independent of SAX-7/L1CAM, MNR-1/Menorin and LECT-2/Chondromodulin II [30,38]. To determine the genetic relationship between *catp-8* and the Menorin pathway, we

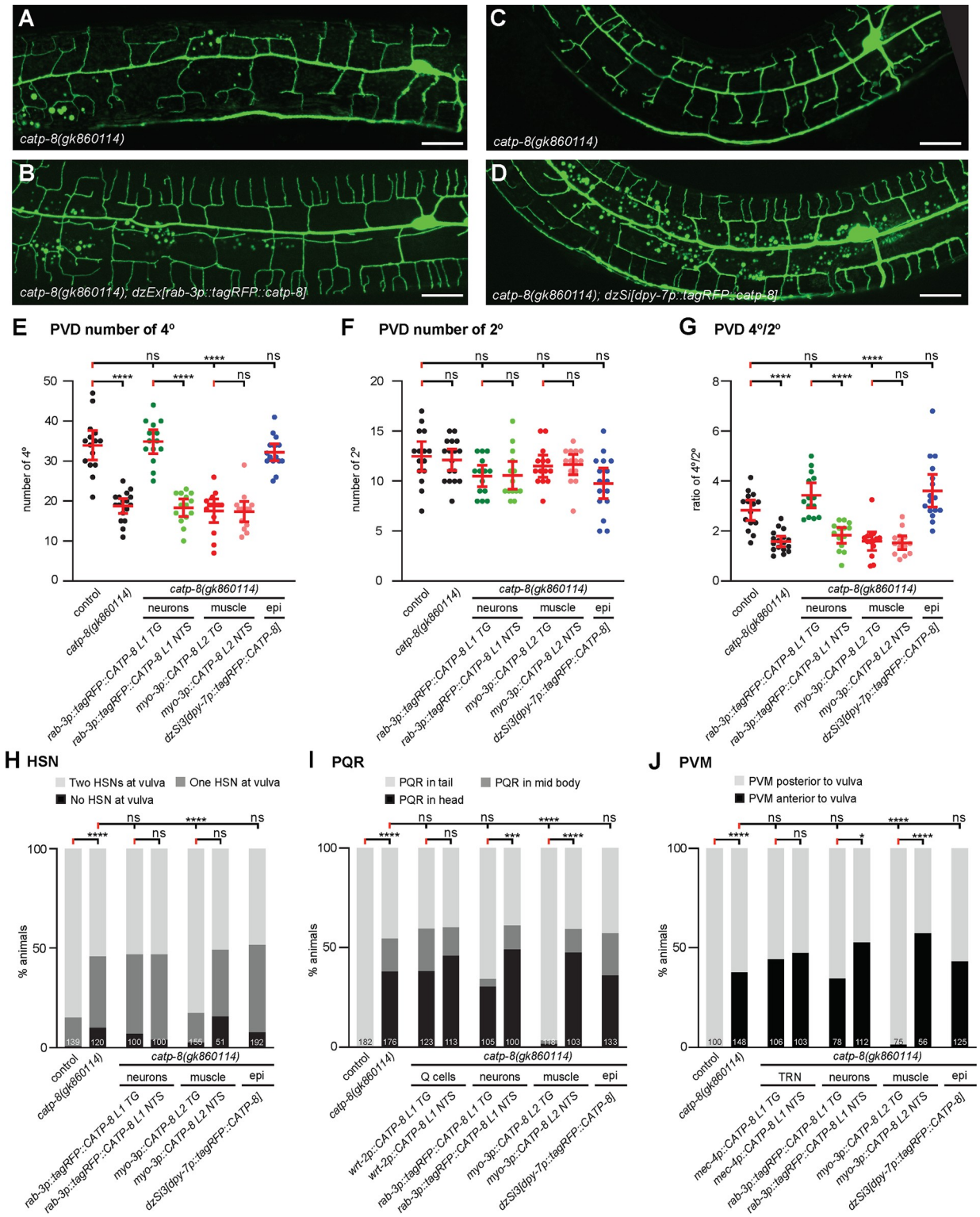

Fig 5. CATP-8/P5A-ATPase can function cell autonomously and non-autonomously during neural patterning. A.—B. Maximum z-projection of confocal images of the PVD::GFP marker *wdIs52* from non-transgenic (A) and transgenic (B) sibling animals carrying the pan-neuronal *catp-8* rescueing array in a *catp-8(gk860114)* mutant background, showing restoration of PVD structure upon neuronal expression. Scale bar = 20μm. C.—D. Maximum z-projection of confocal images of the PVD::GFP marker *wdIs52* from animals without (C) and with (D) single-copy insertion of epidermal *catp-8* rescue under *catp-8* mutant background, showing restoration of PVD structure under epidermal rescue. Scale bar = 20μm. E.—G. Quantification of number of quaternary branches (E), secondary branches (F), and the ratio of quaternary to

secondary branches (G) 100 μm anterior to the PVD cell body in animals of genotypes indicated, showing complete rescue of *catp-8(gk860114)* phenotype when *catp-8* is expressed from pan-neuronal or epidermal promoter, but not muscle promoter. TG: transgenic; NTS: non-transgenic siblings. Data are represented as the mean ± 95% confidence interval. ****, *P<0.0001*, ns, not significant, Kruskal-Wallis test with Dunn's multiple comparisons test. n = 14 animals per genotype. H.—J. Percentage of animals with the indicated migration phenotype of HSN (H), PQR (I) and PVM (J) in the indicated genotypes, showing that all migration phenotypes of *catp-8* were rescued completely when *catp-8* was expressed from muscle, but not when expressed cell-autonomously, pan-neuronally or epidermally. **** $P < 0.0001$, ns not significant, Chi-squared test. Sample size indicated on graph.

https://doi.org/10.1371/journal.pgen.1009475.g005

analyzed double null mutants of *catp-8* and various components of the Menorin pathway using morphometric analyses. We traced and quantified the number and length of secondary, tertiary and quaternary dendrites 100μm anterior to the PVD cell bodies as previously described [30]. With regard to the number of secondary dendrites, we found that the *catp-8* mutant was epistatic in *catp-8; mnr-1* and *lect-2; catp-8* double mutants, i.e. the double mutant resembled the *catp-8* single mutant rather than displaying the increased number of secondary branches observed in the *mnr-1/Menorin* and *lect-2/Chondromodulin II* single mutants (Fig 6A). In double mutants with *dma-1*, *hpo-30* or *tiam-1* the phenotypes were not further enhanced by concomitant genetic removal of *catp-8*. With regard to the number of tertiary branches, we made similar observations, although in some cases the double mutants between *catp-8* and for instance *mnr-1/Menorin*, or *hpo-30/Claudin* appeared phenotypically stronger than the single mutants (Fig 6B). For the number of quaternary branches, double mutants between *catp-8* and genes in the Menorin pathway invariably displayed the stronger phenotype observed in mutants of the Menorin pathway (Fig 6C). We observed similar genetic interactions when investigating the aggregate lengths of secondary, tertiary and quaternary branches (S6 Fig). We conclude that *catp-8* functions in the Menorin pathway and likely within both branches, i.e. the *mnr-1/Menorin*-dependent as well as -independent branches, both of which feed into the DMA-1/LRR-TM receptor in PVD neurons.

CATP-8/P5A ATPase is required for localization of some cell surface transmembrane molecules

The functions of *catp-8* in PVD neurons and the localization to the ER prompted us to test whether the localization or trafficking of two transmembrane molecules, which are expected to transit the ER, is affected in *catp-8* mutants. Specifically, we analyzed the localization of reporters for the single transmembrane receptor DMA-1/LRR-TM (DMA-1::GFP) [39] and the four transmembrane, claudin-like molecule HPO-30/Claudin (HPO-30::tagBFP) [40]. We found that overall DMA-1::GFP expression was noticeably dimmer in *catp-8* mutants (Fig 6D and 6E). When we quantified the fluorescence in the cell body and the primary dendrite we found it strongly reduced in *catp-8* versus control animals (Fig 6F and 6G). Interestingly, the ratio of fluorescence in the cell body versus the primary dendrite was significantly increased (Fig 6H). These observations could be a reflection of reduced trafficking towards the periphery or reduced amounts of DMA-1::GFP/vesicle. To distinguish between these possibilities, we quantified the number of puncta, previously suggested to represent the vesicular fraction of DMA-1::GFP [41,42], in primary and tertiary dendrites of *catp-8* and control animals. We found the number of puncta of DMA-1::GFP in neither primary nor tertiary dendritic branches significantly different in *catp-8* mutant versus control animals (S7B and S7C Fig). We therefore propose that *catp-8* does not serve a function in vesicle trafficking. Instead, *catp-8* may function to facilitate correct membrane localization of DMA-1/LRR-TM. Alternatively, but not mutually exclusive, *catp-8* could serve a role in loading DMA-1::GFP into vesicles.

As previously reported, HPO-30::tagBFP localizes primarily to primary and quaternary dendritic branches [40]. We found that HPO-30::tagBFP fluorescence in distal dendrites

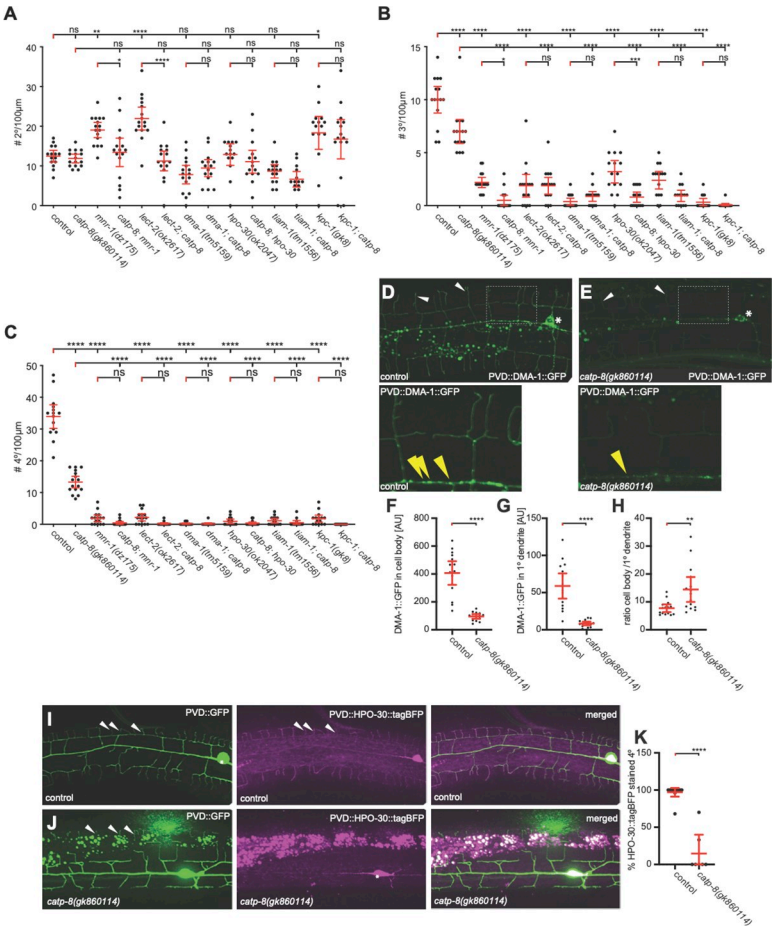

Fig 6. The *catp-8/P5A ATPase* functions with the Menorin pathway during dendrite patterning. A.—C. Quantification of the number of secondary (A), tertiary (B), and quaternary (C) dendrite branches within 100 μm anterior to the PVD cell body in animals of the indicated genotypes. Note that all alleles are molecular or genetic null alleles. Data are represented as the mean ± 95% confidence interval. * $P<0.05$, ** $P<0.01$, *** $P<0.001$, **** $P < 0.0001$ ns not significant; one-sided ANOVA with Tukey's multiple comparison test. n = 15 animals per genotype. D.—E. Maximum z-projection of confocal images and magnified inset of DMA-1::GFP expressed in PVD (*qyIs369*) in a wildtype or *catp-8* mutant background, showing a reduction of DMA-1::GFP puncta in the primary dendrite (yellow arrowheads) in mutant animals. Note also the reduction in overall fluorescence in *catp-8* mutant animals. F.—H. Quantification of DMA-1::GFP signal in cell body (F), and on the primary dendrite 100 μm anterior from the cell body (G) in control and *catp-8* animals. The signal ratio of cell body to primary dendrite is presented in (H). Data are represented as the mean ± 95% confidence interval. ** $P<0.01$, **** $P<0.0001$, Mann-Whitney test. n = 14 animals per genotype. I.—J. Maximum z-projection of apotome images of HPO-30::tagBFP (magenta) expressed in PVD and PVD reporter *wdIs52* (green) in control (I) or *catp-8* mutant animals (J). Note, that as previously reported [40], overexpression of HPO-30::tagBFP in PVD dendrites results in a reduced number of quaternary dendrites possibly due to downregulation of DMA-1/LRR-TM. K. Percentage of HPO-30::tagBFP stained quaternary dendrites 100 μm anterior to the cell body in control or *catp-8* mutant animals, presented as mean ± 95% confidence interval. **** $P<0.0001$, Mann-Whitney test. n = 10 animals per genotype.

https://doi.org/10.1371/journal.pgen.1009475.g006

appeared reduced in *catp-8* mutant animals (Fig 6I and 6J). Although HPO-30::tagBFP expression in the cell body did not seem visibly different, HPO-30::tagRFP fluorescence in quaternary dendrite branches was strongly reduced in *catp-8* mutant versus control animals (Fig 6K). Yet, the number of HPO-30::tagRFP puncta in the PVD primary branch remained unaffected, implying again that trafficking of HPO-30::tagBFP does not require *catp-8* function (S7D Fig).

Because epidermal expression of *catp-8/P5A-ATPase* could rescue PVD defects in *catp-8* mutant animals, we tested, whether another conserved transmembrane cell adhesion molecule SAX-7/L1CAM, which functions in the epidermis to shape PVD dendrites, is affected in *catp-8* mutant animals. We found that SAX-7::GFP localization appears qualitatively and quantitatively unchanged in *catp-8* mutants compared to control animals, or in animals that overexpressed tagRFP::CATP-8 transgenically in the epidermis (S7E and S7F Fig). Similarly, localization of the secreted LECT-2/Chondromodulin II was not affected in *catp-8* mutants (S7G Fig). We conclude, *catp-8/P5A-ATPase* function is required for the regulation and localization of some but not all transmembrane proteins.

CATP-8/P5A ATPase functions with the Wnt signaling pathway to control neuronal migrations

Our studies show that *catp-8* is required for both embryonic and postembryonic neuronal migrations, including the anteriorly directed embryonic migrations of HSN neurons and the posteriorly directed postembryonic migrations of the Q cell descendants PVM and PQR. Both of these cell migrations are genetically well-described and depend on, among other pathways, Wnt signaling [10,11,13]. Briefly, the *egl-20/Wnt* ligand is expressed in posterior tissues, including body wall muscle [43,44], is believed to form a gradient [45] and to function through the G-protein coupled receptor *mig-1/Frizzled* in HSN neurons to mediate HSN migration [46]. While other Wnts and frizzled receptors play smaller, largely redundant roles in HSN migration [13], most functions appear to be mediated by the MIG-1/Frizzled receptor in HSN neurons, because a *mig-1; egl-20* double mutant does not display more severe defects in HSN migration than the single mutants [47]. To investigate the genetic relationship between *catp-8/P5A-ATPase* and Wnt signaling, we therefore created a double null mutant between *catp-8* and *mig-1*. We found that the HSN migration phenotype in *mig-1; catp-8* double mutant animals was not enhanced compared to the more severe of the single mutants (*mig-1/Fz*) (Fig 7A). This suggests that *catp-8* functions genetically in a pathway with *mig-1/Frizzled* and, by inference, Wnt signaling.

The migration of Q cell descendants occurs in two phases [11]. In an initial phase, the QL and QR cells, both of which are located laterally on either side of the animals, are polarized and migrate about the distance of one cell diameter over the posteriorly and anteriorly located epidermal blast cells, respectively (Figs 7B and S7A). This is followed by a second phase, in which the QL and QR cells migrate further posteriorly and anteriorly, respectively, while undergoing the stereotyped cell divisions [34](Fig 2A). The first phase is controlled by at least three partially redundant genetic pathways, which are defined by genes encoding: (1) the transmembrane cell adhesion molecule UNC-40/DCC (Deleted in Colorectal Cancer)[48], (2) the transmembrane protein MIG-21 and the conserved, putative C-mannosyl transferase DPY-19/DPY19L [48–50], and (3) the cadherin proteins CDH-3, CDH-4, and the LAR-like receptor tyrosine phosphatase PTP-3/LAR [51–53]. Mutations in any of these genes result in defects in the initial polarization and, consequently, migration. In contrast, we find that initial polarization and migration of QL and QR cells proceeds normally in *catp-8* null mutant animals, suggesting that *catp-8* functions primarily during the second phase of migration (Figs 7B and S7A). Consistent with this interpretation, we found that *unc-40; catp-8* double mutants exhibited a more severe phenotype than either single mutant alone (Fig 7C–7E). Similar results were found in *mig-21; catp-8* and *ptp-3; catp-8* double mutant animals, which also showed a more severe phenotype compared to the single mutants (Fig 7C–7E). We conclude that *catp-8* serves no individual role during the first phase of Q cell migration, but rather functions during the second phase of Q cell migration.

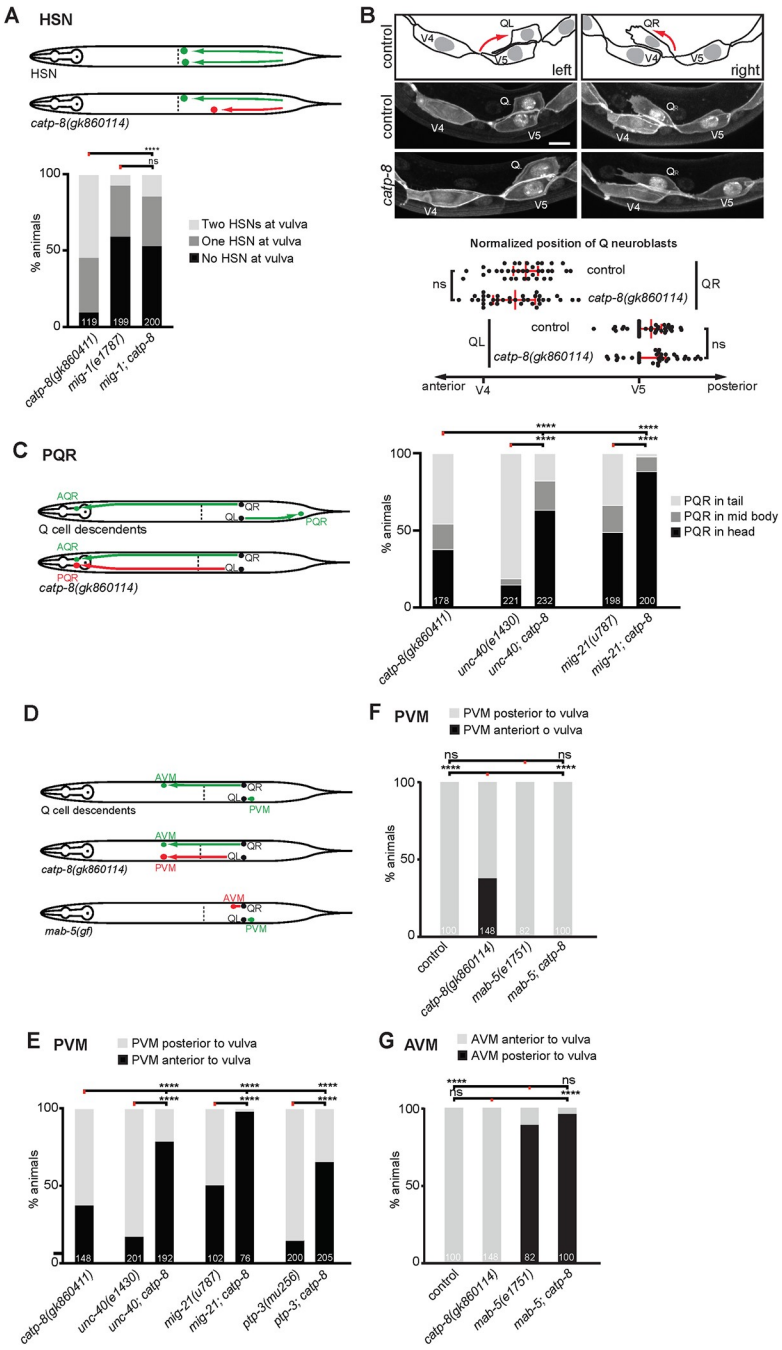

Fig 7. Genetic interactions of *catp-8/P5A* ATPase during cell migrations. A. Schematics depicting normal HSN migration (upper panel) and HSN migration defects (lower panel), and quantification of HSN migration defects in the genotypes indicated. Percent animals are shown with neurons in the wild type position (light grey bars), partially incomplete migration (dark grey bars) and completely failed migration (black bars). Pairwise statistical significance was calculated using Chi-squared test or Fisher exact test. **** $P \leq 0.0001$, ns not significant. Sample size indicated on graph. B. Schematic, images and quantification of the relative position of initial Q neuroblast migration in the genotypes indicated, imaged 4.5 hours after hatching. Scale bar = 5 μm. Data are represented as the mean ± 95% confidence interval. ns not significant; Mann-Whitney test. n = 35 animals per genotype. C. Schematics depicting normal PQR migration (upper panel) and migration defects (lower panel), and quantification of PQR migration defects in the genotypes indicated. Percent animals are shown with neurons in the wild type position (light grey bars), partially incomplete migration (dark grey bars) and completely failed migration (black bars). Pairwise statistical significance was calculated using Chi-squared test or Fisher exact test. **** $P \leq 0.0001$. Sample size indicated on graph. D. Schematics depicting normal AVM and PVM migration (upper panel) and migration defects (middle and lover

panels) in the genotypes indicated. E. Quantification of PVM migration defects in the genotypes indicated. Percent animals are shown with neurons in the wild type position (light grey bars), and failed migration (black bars). Pairwise statistical significance was calculated using Chi-squared test or Fisher exact test. **** $P \leq 0.0001$. Sample size indicated on graph. F.–G. Quantification of PVM (F) and AVM (G) migration defects in the genotypes indicated. Percent animals are shown with neurons in the wild type position (light grey bars), and failed migration (black bars). Pairwise statistical significance was calculated using Chi-squared test or Fisher exact test. **** $P \leq 0.0001$, ns not significant. Sample size indicated on graph.

https://doi.org/10.1371/journal.pgen.1009475.g007

We next focused our analysis on the second phase of migration and in particular on AVM and PVM migrations. The *mab-5/HOX-C* antennapedia-like homeobox transcription factor is necessary and sufficient in QL cells after the initial polarization to mediate the second phase of their posterior migration [54] and is activated in response to the *egl-20/Wnt* morphogen that is expressed in posterior tissues [43]. Similar to loss of *catp-8*, loss of *mab-5* results in QL cell migration defects, where QL cell descendants migrate in an anterior rather than posterior direction [54]. Because the *mab-5* mutant phenotype is essentially fully penetrant, we could not test for possible enhancement in a *mab-5; catp-8* double mutant. However, in a *mab-5(gf)* gain of function allele *mab-5* is activated in both QL and QR cells. Migration of the QL descendants is not affected in the *mab-5(gf)* gain of function mutants, whereas QR descendants fail to migrate in an anterior direction [54]. We therefore tested the epistatic relationship between the *mab-5(gf)* allele and the *catp-8* loss of function mutant. We found that the aberrant anterior migration of the QL descendant PVM in *catp-8* single mutants was completely suppressed in a *mab-5(gf); catp-8* double mutant (Fig 7D and 7F). In contrast, the migration defects of QR descendants in a *mab-5(gf)* remained unaffected by concomitant loss of *catp-8* (Fig 7D and 7G). Thus, *catp-8/P5A-ATPase* functions upstream of or in parallel to the *mab-5/HOX-C* homeobox transcription factor.

Discussion

In this study we describe multiple functions of the *catp-8/P5A-ATPase* in metazoan development. Specifically, we show that *catp-8* is required for different aspects of nervous system development, including axonal guidance, dendrite patterning and neuronal migrations. A reporter for CATP-8/P5A-ATPase is expressed in the ER of most if not all tissues and can function both cell-autonomously and non-autonomously during neuronal development. Genetically, *catp-8/P5A* functions in multiple pathways, including the conserved Menorin pathway during dendrite development and Wnt signaling during neuronal migrations. We find a substantial degree of genetic redundancy with different developmental pathways, suggesting that *catp-8/P5A-ATPase* may serve diverse, yet specific functions in different cellular contexts Lastly, *catp-8/P5A-ATPase* is necessary to correctly localize reporters for some but not all transmembrane proteins.

Functional redundancy of catp-8/P5A-ATPase in neuronal patterning

Not all neurons are affected by loss of *catp-8* function. For example, the PVD somatosensory neurons require *catp-8* for the elaboration of dendritic trees, but the dendrites of amphid sensory neurons seem unaffected. Similarly, axonal guidance or extension of HSN and D-type motor neurons requires *catp-8* function, whereas guidance of PVQ axons or DA/DB motor neurons appears independent of *catp-8*, respectively. It is interesting to note that PVQ and HSN (but also D-type and DA/DB motor neurons to some extent) make similar navigational choices, are part of the same fascicles and depend on similar axon guidance pathways, such as Netrin signaling or Slit/Robo signaling [46,55,56], although we cannot exclude that the extracellular or signaling environment is distinct at different times during development. It should

be noted that Wnt signaling is also required for correct axon guidance of both HSN and PVQ axons at the midline [46,57] and, at least for the latter cellular context, has been shown to function in parallel with Netrin signaling [57]. A possible explanation is that different genetic redundancies for *catp-8* exist in different cells; in other words, in some cells, *catp-8* may serve unique roles for which no functional alternative to *catp-8* exists whereas in other cells *catp-8* has functions that can be partially served by other genes. Such genes could be the related *catp-6* or *catp-7* ATPases, although at least in PVD patterning they play no redundant roles [23]. Alternatively, the molecules that are required for development of a given cell may be distinct in different neurons, such that some neurons depend on more or less proteins requiring *catp-8* function.

Transgenic rescue experiments suggest both cell-autonomous and non-autonomous functions for *catp-8*. For example, PVD can develop normally with *catp-8/P5A-ATPase* function present in either neurons or the epidermis. This finding is in contrast to findings by Feng et al. who could rescue *catp-8* defects by transgenic expression of *catp-8* in neurons, but not in muscle or the epidermis [23]. One possible explanation for this discrepancy is different levels in transgene expression (we use a single copy transgenes for epidermal expression whereas Feng et al. utilized multi copy transgenes [23]). This hypothesis is supported by the fact that the Menorin pathway is known to be dosage sensitive and can be both positively and negatively regulated [58,59].

In contrast to this tissue redundancy, the migration defects of Q cell descendants are rescued only by non-autonomous expression of *catp-8* in muscle, but not by expression in neurons or other tissues. These results strongly argue for a non-autonomous function of *catp-8/P5A-ATPase* in muscle during migration. However, no transmembrane proteins are known to function from muscle in Q cell migration, although muscle is clearly important, as both the RNA-Binding Protein ETR-1/CELF1 and the extracellular matrix protein SPON-1/F-spondin can function in muscle cells to mediate Q cell migration [60,61]. It is therefore tempting to speculate that secretion of the EGL-20/Wnt ligand could be regulated by *catp-8/P5A-ATPase*

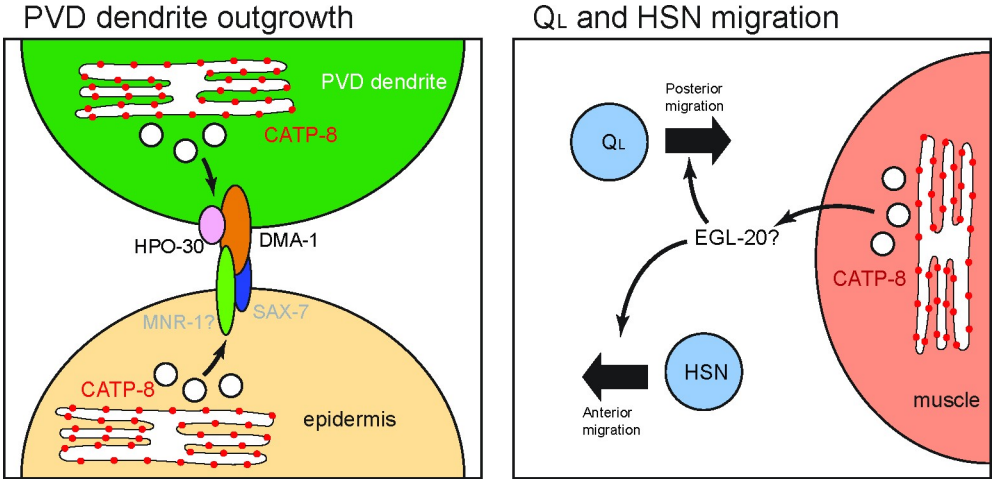

Fig 8. Graphical Model of CATP-8 functions. CATP-8 is associated with the endoplasmic reticulum and regulates or facilitates the secretary pathway. In the case of PVD dendritic outgrowth, CATP-8/P5A-ATPase is proposed to ensure the expression and localization of DMA-1 and HPO-30 in PVD, as well as transmembrane factors from the epidermis, of which one candidate is MNR-1. In the case of QL neuroblast and HSN migration, our results strongly suggest that CATP-8 ensures the sufficient secretion of the Wnt ligand EGL-20, which is needed for the posterior migration of QL neuroblasts, and the anterior migration of HSN neurons.

https://doi.org/10.1371/journal.pgen.1009475.g008

(Fig 8). First, we found, that during HSN migration (and possibly also Q cell migration), Wnt signaling functions in concert with the *catp-8/P5A-ATPase*. Second, EGL-20/Wnt has been shown to be expressed from posterior body wall muscle among other posterior tissues [44,45]. Third, the cellular migrations that are affected in *catp-8/P5A-ATPase* mutant animals (PVM, PQR, HSN) are all dependent on *egl-20/Wnt* whereas cell migrations that are independent of *catp-8/P5A-ATPase* (ALM, coelomocytes) are also independent of *egl-20/Wnt* [13]. Lastly, a *mab-5(gf)* mutant rescues the *catp-8/P5A-ATPase* mutant and is therefore likely downstream of *catp-8* –just as *mab-5* is downstream of *egl-20/Wnt* [43]. Further experiments are needed to definitively establish whether and how EGL-20/Wnt secretion or localization is dependent on *catp-8/P5A-ATPase* function.

Substrates of the CATP-8/P5A-ATPase

Previous studies in yeast and plants suggested various roles for P5A-ATPases, such as functions in phosphate homeostasis and male gametogenesis [18–20], phospholipid and sterol homeostasis [21] and targeting of mitochondrial outer membrane proteins [22]. Therefore, which functions P5A ATPases may serve in metazoans remains a major question. Here, we provide genetic evidence that *catp-8/P5A-ATPase* is required for the localization of sufficient amounts of the DMA-1/LRR-TM receptor in the membrane of higher order PVD dendrites during morphogenesis. Similarly, the four transmembrane protein HPO-30/Claudin, which also functions in PVD neurons during dendrite patterning [62] requires *catp-8* to be correctly localized to distal, higher order dendrites. Importantly, the number of vesicles containing the respective reporters and, which are presumed to represent endocytic/transport vesicles [41,42] along the dendritic branches, remain unaffected. Intriguingly, localization of the conserved SAX-7/L1CAM cell adhesion molecule in either neurons or the epidermis is not obviously affected. Therefore, *catp-8* may be involved in the insertion/localization of certain transmembrane proteins but not others to the plasma membrane (Fig 8). These findings are consistent with another recent study showing similar effects on DMA-1::GFP [23,24], although it was also reported by Qin et al. that the levels of a HPO-30 reporter remained unchanged [24]. A possible explanation for this discrepancy is that we measured fluorescence in distal dendrites rather than the cell body [24]. The findings of a role for the *catp-8/P5A ATPase* in the localization of some cell surface proteins is seemingly at odds with two other studies in yeast and *C. elegans* suggesting that P5A-ATPases primarily maintain ER homeostasis by functioning as dislocases to remove mislocalized mitochondrial proteins [24,25]. However, several arguments can be made that P5A-ATPases serve additional functions beyond removing mislocalized mitochondrial proteins. First, genetic manipulations in *C. elegans* that suppress ER defects in PVD due to mislocalized DRP-1/Drp1 mitochondrial fission protein to the ER in *catp-8* mutants, fail to restore the correct dendritic morphology [24] suggesting that *catp-8/P5A-ATPase* serves additional functions beyond maintaining ER integrity to mediate PVD morphogenesis. Second, proteomic studies in HeLa cells found not only the levels of mitochondrial, but also other transmembrane and secreted proteins changed in ATP13A1/P5A-ATPAse mutant cells. For example, a number of secreted growth factors, including the platelet derived growth factor D (PDGFD) or transforming growth factor beta (TGFB) as well as axon guidance molecules such as ephrin A5 (EFNA5), to name but a few, were significantly reduced in abundance upon loss of ATP13A1 catalytic activity [25]. In the context of these studies, our findings argue for a more diverse, yet likely specific role for *catp-8* in the localization of certain transmembrane proteins and regulation of secreted proteins (Fig 8). Further experiments will be required to delineate the full spectrum of genetic and biochemical functions of P5A-type ATPases.

Materials and methods

C. elegans strains and genetics

All *C. elegans* strains were grown on nematode growth medium plates with *E. coli* (OP50) as a food source as described [63], usually at 20˚C unless otherwise specified. Strains used in this work can be found in S1 Table. The *catp-8* alleles *dz224* and *gk860114* were backcrossed four and three times, respectively, prior to further analysis.

Molecular cloning of *catp-8(dz224)*

Using a combination of Hawaiian SNP mapping and sequencing [26] the allele *dz224* was localized to a region between 8Mb and 13Mb on LG IV, which was further refined by deficiency mapping to between 10.2Mb and 12Mb (S1 Fig). This 1.8Mb interval comprised 7 non-synonymous missense mutations and one non-sense mutation in *catp-8*, which was confirmed by Sanger sequencing: an A to a T transversion at position 11,479,010 on LG IV (WB270), resulting in an ochre premature stop codon after Y55 in *C10C6.6* (*catp-8*). We found that *catp-8(gk860411)* failed to complement *dz224*, further suggesting that both alleles are affecting the same gene.

Molecular biology and transgenesis

Cloning of all constructs were carried out using standard molecular biology methods. A list of primers used can be found in S2 Table. For a list of plasmids used and detailed descriptions of constructs see S3 and S4 Tables. All extrachromosomal arrays were generated by injecting a mixture of the desired plasmids with *pBluescript* to a final concentration of 100 ng/μl of DNA. A detailed list of all the extrachromosomal transgenic lines generated can be found in S5 Table.

For CRISPR/Cas9 mediated genome editing, appropriate guide RNA sites were selected using IDT Cas9 crRNA design tool and, oligos in the general form of TAATACGACTCACTA TA(gRNA)GTTTTAGAGCTAGAAATAGCAAG were ordered, where (gRNA) is the 20nt of the guide RNA sequence before the PAM motif, optimized for T7 promoter transcription. These oligos were used in PCR reactions as a forward primer in conjunction with the universal reverse primer AAAAGCACCGACTCGGTG (oLT337) to generate sgRNA transcription templates from pDD162 (containing the sequence of tracrRNA). sgRNA was then transcribed from this template using the HiScribe T7 *in-vitro* transcription kit (NEB) and purified with the Monarch RNA cleanup kit (NEB). The resulting sgRNA was used in an injection mix at 20 ng/μl per sgRNA, together with 250 ng/μl of Alt-R Cas9 endonuclease (IDT) and repair templates (100 ng/μl for single-strand oligos, 200 ng/μl for PCR products or plasmids). Injection and CRISPR efficiency were monitored through a Co-CRISPR strategy with *dpy-10(cn64)* or *unc-58(e665)* conversions, or through *rol-6(su1006)* co-injection markers [64]. A list of all genome-edited strains and detailed methodology can be found in S6 Table.

Scoring of migration phenotypes

All worms were immobilized using 1 mM levamisole and mounted on 4% agarose pads for phenotypic analysis.

AQR/PQR migrations were scored in *wdIs52 (Is[F49H12.4p*::*GFP])* in L2 to young adults with a Plan-Apochromat 10x/0.25 objective on a Zeiss Axioimager Z1. Cells were considered in the head if anterior to the intestine, in the tail if posterior to the intestine, and in the mid body otherwise. AVM/PVM migrations were scored in *zdIs5 (Is[mec-4p*::*GFP])* in L4 to young adults with a Plan-Apochromat 10x/0.25 objective on a Zeiss Axioimager Z1. Cells were scored

based on their relative position (anterior or posterior) to the vulva. HSNs migrations were scored in *dzIs75 (Is[kal-1p9*::*GFP])* in adult worms with a Plan-Apochromat 16x/0.5 objective on a Zeiss Axioimager Z1. Cells were considered to be at the vulva if the cell bodies were positioned less than or equal to an egg's length posterior to the vulva. ALM was scored in *zdIs5 (Is [mec-4p*::*GFP])* in synchronized L1 animals. Animals are imaged using a Plan-Apochromat 10x/0.25 objective on a Zeiss Axioimager Z1 Apotome. Using ImageJ, the distance of the more anterior cell body from the nose was measured and divided by the total length of the animal. Coelomocytes were scored in *dzEx2140* at the L4 to young adult stage with a Plan-Apochromat 16x/0.5 objective on a Zeiss Axioimager Z1. Coelomocytes were considered to be in the head region if in the anterior quarter of the worm.

Scoring of axon pathfinding

HSN axon guidance at the ventral midline was scored in *dzIs75* or *mgIs71* at the L4 to adult worms stage with a Plan-Apochromat 40x/1.3 objective on a Zeiss Axioimager Z1. Crossover defects of axons were scored if any portion of the axons of HSNL and HSNR were touching. DD/VD neurons were scored in *juIs76* at the L4 to adult worm stage with a Plan-Apochromat 40x/1.3 objective on a Zeiss Axioimager Z1. Axon guidance was categorized into two measurements, L/R choice and gaps in the dorsal or ventral cord. For L/R choice, any worm with 1 or more axons found on the opposite side of the stereotyped location was counted as having an L/R choice defect as indicated. Additionally, any worm with a visible discontinuation of the dorsal and/or ventral cord between any two neurons (gaps) was considered to have a dorsal and/or ventral cord defect respectively. DA/DB motor neurons were scored in *evIs82b* at the L4 to adult stage with a Plan-Apochromat 40x/1.3 objective on a Zeiss Axioimager. Axon guidance was categorized into two measurements, L/R choice and gaps in the dorsal or ventral cord. For L/R choice, any worm with 1 or more axons found on the opposite side of the stereotyped location was counted as having an L/R choice defect. Any worm with a visible discontinuation of the dorsal and/or ventral cord between any two neurons (gaps) was considered to have a dorsal or ventral cord defect, respectively. AIY axonal morphology was scored with *mgIs32* at the L4 to adult stage with a Plan-Apochromat 16x/0.5 objective on a Zeiss Axioimager Z1. Cells were considered to be overbranching if an additional protrusion off of the cell body at least the length of the cell body was present. PVQ axonal guidance was scored in *oyIs14* at the L4 to adult stage with a Plan-Apochromat 16x/0.5 objective on a Zeiss Axioimager Z1. Crossover defects were counted if any portion of the axons of PVQL and PVQR anterior to the vulva were not visibly separable. For DiI staining**, w**ell-fed adult worms were washed from plates with 1 mL M9, pelleted, resuspendend in 1 mL M9 before 5 μL of DiI stock solution (2 mg/mL DiI (Molecular Probes, #D282) in dimethyl formamide) was added. Animals were incubated with light shaking for 3 hours, spun and washed with M9 two times, followed by transfer to fresh plates. After 30 minutes recovery, animals were immobilized in 1 mM levamisole and neuronal processes were assessed for defects and imaged with a Plan-Apochromat 40x/1.3 or 63x/1.4 objective on a Zeiss Axioimager Z1 Apotome.

Fluorescent microscopy and quantification

PVD morphometric analysis. Fluorescent images were captured in live *C. elegans* at the L4 larval stage using a Plan-Fluor Nikon 40x/1.3x on a Nikon CSU-W1 Spinning Disk Confocal. At least 15 L4 larval animals were scored per genotype. Optical sections were collected and maximum intensity projections adjusted for optimal contrast to resolve detailed morphology were used for further analysis. For tracing, the 100 μm section of the primary branch anterior to the cell body was used for morphometric analyses using the NeuronJ plugin of the FIJI

software. Branches were defined as follows: 2˚ dendritic branches as any neurite branching out of the primary dendrite; 3˚ branches as neurites branching at the end of a 2˚ branch in proximity to the tertiary line along the border of outer body wall muscles and the lateral epidermis; 4˚ dendritic branches as those originating from 3˚ dendritic branches and extending towards the dorsal or ventral nerve cords, respectively.

DMA-1::GFP quantifications. All DMA-1::GFP fluorescent images were captured in strains containing *qyIs369* at the L4 larval stage using a Plan-Fluor Nikon 60x/1.4x objective and GFP filter setting on a Nikon CSU-W1 Spinning Disk Confocal with identical imaging parameters and appropriate z-stack. Fluorescence measurements of the z-projected image were subsequently performed in ImageJ as follows. For Intensity of GFP in the PVD cell body an outline of the cell body was drawn as Region of Interest (ROI) and the average signal in the ROI was quantified. An ROI of the same shape was placed outside of the cell body to measure the background signal, which was subtracted from the fluorescent signal. For the intensity of GFP in the PVD primary dendrite, the primary dendrite was traced for 100 μm anterior to the cell body, and an ROI was defined as 10 pixels (= 1.6 μm) thick along the traced line, where the average signal in the ROI was quantified. A ROI of the same size was placed next to the dendrite to measure the background signal, which was subtracted from the fluorescent signal. The number of puncta within 100 μm of the primary dendrite anterior to the cell body were counted manually.

HPO-30::tagBFP quantification. All HPO-30::tagBFP fluorescent images were captured in strains containing *dzEx2140* and *wdIs52* at the L4 larval stage using a 40x/1.3 objective on a Zeiss Axioimager Z1 Apotome with identical imaging parameters for tagBFP and GFP filter setting, and appropriate z-stacks. Quantification of the z-projected images were subsequently performed in ImageJ as follows. For the percentage of quaternary dendrites containing HPO-30::tagBFP, the number of quaternary branches with visible tagBFP signal within 100 μm anterior to the cell body were counted in the tagBFP channel, then divided by the number of quaternary dendrites as imaged in the GFP channel. For the number of HPO-30::tagBFP puncta, quantification was performed by manually counting the puncta within 100 μm anterior to the cell body.

SAX-7::GFP and LECT-2::mNG imaging:. Fluorescent images for the strains containing the *ddIs290* fosmid based SAX-7::GFP reporter or *dz249[lect-2*::*GFP]* endogenous knock-in were captured at the late L4 larval stage using a Plan-Apochromat 40x/1.3 objective on a Zeiss Axioimager Z1 Apotome at an exposure time of 151 ms, followed by appropriate z-stacks. Neuronal and epidermal patterning were assessed, and the PVD phenotype was observed in a *dzIs53* background.

Colocalization assay of subcellular compartment markers. L4 animals carrying *dzSi3* and single-copy insertions of GFP subcellular compartment markers were imaged using a Plan-Fluor Nikon 60x/1.4x objective on a Nikon CSU-W1 Spinning Disk. Single planes from a confocal image stack in which both the *catp-8* and organellar reporters were clearly visible were manually thresholded, then analyzed using the Correlation Plot application in Metamorph 7.7 to establish a Pearson's Correlation Coefficient for each image pair.

Analysis of Q neuroblast polarization. Animals carrying the *heIs63* transgene were synchronized and imaged 4.5 hours after hatching using a Plan-Fluor Nikon 100x/1.4x objective on a Nikon CSU-W1 Spinning Disk Confocal, before the first cell division of the Q neuroblast. The normalized position of the Q neuroblast was calculated by first drawing a straight line between the nuclei of V4 and V5, then the perpendicular location of nuclei of Q neuroblasts on the line was noted. The normalized position was calculated by subtracting the distance between the nuclei of V5 and Q neuroblasts (negative if posterior to V5) from that between the

nuclei of V4 and Q neuroblasts (negative if anterior to V4) and divided by that between the nuclei of V4 and V5.

Statistical analysis

All statistical analyses were performed using the Prism 9 Statistical Software suite (GraphPad). All pairwise migration phenotypes are analyzed with Fisher exact test when applicable, or Chi-squared test as indicated. All comparisons of averages/proportions are analyzed with one-way ANOVA with Tukey correction, the Kruskal-Wallis test, the Mann-Whitney test, or the Z-test as applicable.

Supporting information

S1 Table. List of strains used. S1 Table lists all strains that were used during this study, including strain names and genotypes.
(XLSX)

S2 Table. Primers and oligos. S2 Table lists all primers and oligos that were used during this study, including name, sequence and their applicationb.
(XLSX)

S3 Table. Plasmids generated in previous papers. S3 Table lists all plasmids that were used during this study and had been previously described.
(XLSX)

S4 Table. Plasmids generated for this paper. S4 Table lists all plasmids that were generated and used during this study.
(XLSX)

S5 Table. List of Extrachromosomal arrays generated. S5 Table lists all extrachromosomal transgenes that were generated and analyzed during this study.
(XLSX)

S6 Table. CRISPR edited strains generated. S6 Table lists information regarding alleles, strain names and reagents that were generated and used, respectively, during this study for CRISPR/Cas9 mediated genome engineering.
(XLSX)

S1 Fig. Mapping and auxiliary genetics. A. Frequency plot of N2 SNPs from whole genome sequencing results as per Hawaiian SNP mapping [26], indicating *dz224* lesions reside between 6 Mbp and 13 Mbp on linkage group (LG) IV. Deficiencies covering the region are indicated below (green, complementation of *dz224*; red non-complementation of *dz224*), demonstrating that *dz224* lesions lies between 10,202,993, and 12,011,007 bp, the physical positions of the last known genes inside of *eDf19* and the first one outside of *mDf7*, respectively. The table below lists lesions detected within this range, with *catp-8* containing the only stop-gain mutation. B.—E. Quantification of the number of secondary branches that reach the tertiary line where muscle and epidermis abut (B)(i.e. excluding ectopic stunted secondary branches), aggregate length of all secondary (C), tertiary (D), and quaternary (E) dendrite branches 100 μm anterior to the PVD cell body in the genotypes indicated. Data are represented as the mean ± 95% confidence interval. Statistical significance was calculated using one-sided ANOVA with Tukey's multiple comparison test. * $P \leq 0.05$, *** $P \leq 0.001$, **** $P \leq 0.0001$, ns not significant. F. Complementation assay tallying the percentage of animals with PVD defects. Note that there is non-complementation between *dz224* and *catp-8(gk860114)*, recessiveness of *dz224* and

catp-8(gk860114), and absence of maternal effects. G. Quantification of the number of quaternary and secondary branches, and the ratio of quaternary to secondary branches 100 μm anterior to the PVD cell body in *catp-8(gk860114)* and *catp-8(gk860114)/mDf7* transheterozygous animals. No enhancement was observed in the transheterozygous genotype, showing that *gk860114* behaves as a genetic null allele. Data are represented as the mean ± 95% confidence interval. ns not significant, Kruskal-Wallis test with Dunn's multiple comparisons test. n = 14 animals per genotype. H. Body length of wildtype and *catp-8(gk860114)* L1 larval animals, measured and presented as mean ± 95% confidence interval. ns not significant. Statistical significance was calculated with an unpaired t-test. I. Fraction of *catp-8* homozygous mutant animals presenting PQR migration defects originating from homozygous or heterozygous *catp-8* mutant parents. PQR migration is completely normal in F1s originating from heterozygous animals, indicating a maternal contribution of *catp-8* in PQR migration. Homozygosity of animals was determined by the PVD phenotype, which is not maternally rescued. J. Fraction of descendants from *catp-8(gk860114)* heterozygous animals with HSN migration defects, suggesting the absence of maternal effects. * $P \leq 0.05$, Fisher exact test.
(TIFF)

S2 Fig. Additional neuronal phenotypes in catp-8 mutant animals. A.—B. Maximum z-projection confocal images of DA/DB cholinergic motor-neurons (visualized by *evIs82b (Is[unc-129p*::*GFP])* of wildtype (A) and *catp-8* mutant animals (B). No difference between the genotypes were observed. Lateral views, ventral up, anterior to the left. C.—D. Maximum z-projection confocal images of D-type GABAergic motor-neurons (visualized by *juIs76(Is[unc-25p*::*GFP]*) of wild type (C) and *catp-8* mutant animals (D). Occasional gaps caused by underextension of neurites can be observed in *catp-8* mutant animals. Lateral views, dorsal up, anterior to the left. E.—F. Maximum z-projection confocal images of AIY interneurons (visualized by *mgIs32 (Is[ttx-3p*::*GFP]*) in wildtype (E) and *catp-8* mutant animals (F). No difference between the genotypes was observed. Lateral views, dorsal up, anterior to the left. G.—J. Maximum z-projection apotome images of DiI stained phasmid and amphid sensory neurons, respectively in wildtype (G,I) and *catp-8* mutant animals (H,K). No difference between the genotypes was observed. Ventral views, anterior to the left. Lateral views, dorsal up, anterior to the left. K.—N. Maximum z-projection confocal images of PVQ interneurons (visualized by *oyIs14 (Is[sra-6p*::*GFP])* (K,L) and HSN motor-neurons (visualized by *dzIs75 (Is[kal-9p*::*GFP]*) (M,N) in wildtype and *catp-8* mutant animals. No defects were observed in PVQ axons at the midline, but HSN neurons showed a significant number of midline cross overs in *catp-8* mutant animals (see also Table 1). Ventral views, anterior to the left.
(TIFF)

S3 Fig. A catp-8 transcriptional reporter is widely expressed. A.—E. Maximum z-projection confocal images of an embryo (A), L2 larval animal (B), L3 larval animal (C-D) and L4 larval animal (E) carrying the *catp-8p* promoter GFP reporter fusion array *dzEx2101*. *dzEx2101* exhibits a high degree of mosaicism, resulting in staining of different tissues across the population, including muscle, intestine, pharynx, and some unidentified neurons.
(TIFF)

S4 Fig. Different organelles are not visibly affected in *catp-8* mutants. Confocal images of single copy insertion transgenes of epidermally expressed organellar reporters in *catp-8 (gk860114)* mutant and wild type animals, for ER/endoplasmic reticulum (*pwSi82 [Phyp-7*::*VIT2ss*::*oxGFP-KDEL]*), cis/medial Golgi (*pwSi202 [Phyp7*::*AMAN-2*::*mNG;HYG-R]*), early endosomes (*pwSi145 [Phyp7*::*mNG*::*RAB-5;HYG-R]*), late endosomes and lysosomes *pwSi140 [Phyp7*::*mNG*::*RAB-7;HYG-R]*), autophagosomes (*pwSi144 [Phyp7*::*mNG*::*LGG-1;HYG-R])*,

and lysosomes (*pwSi205 [Phyp7*::*LMP-1*::*mNG;HYG-R]*).
(TIFF)

S5 Fig. Complete data of cell specific rescue experiments. A.—C. Quantification of the number of quaternary branches (A), secondary branches (B), and the ratio of quaternary to secondary branches (C) 100 μm anterior to the PVD cell body in animals of all extrachromosomal rescue lines tested. TG: transgenic animals, NTS: non-transgenic siblings. Data are represented as the mean ± 95% confidence interval. **** $P < 0.0001$, ns not significant, Kruskal-Wallis test with Dunn's multiple comparisons test. n = 14 animals per genotype. D.—E. Percentage of animals with the indicated migration phenotype of PVM (D) and PQR (E) for all extrachromosomal rescue lines tested. TG: transgenic animals, NTS: non-transgenic siblings. **** $P <$ 0.0001, ns not significant, Chi-squared test. n > 75 animals per genotype.
(TIFF)

S6 Fig. Additional morphometric data of genetic double mutant analysis. A.—C. Quantification of the aggregate length of secondary (A), tertiary (B), and quaternary (C) dendrite branches within 100μm anterior to the PVD cell body in animals of the indicated genotypes. Note that all alleles are molecular or genetic null alleles. Data are represented as the mean ± 95% confidence interval. * $P < 0.05$, ** $P < 0.01$, *** $P < 0.001$, **** $P < 0.0001$ ns not significant; one-sided ANOVA with Tukey's multiple comparison test. n = 15 animals per genotype.
(TIFF)

S7 Fig. Loss of *catp-8* does not affect DMA-1::GFP or HPO-30::tagBFP puncta, SAX-7::GFP and LECT-2::mNG expression and distribution, or initial Q neuroblast morphologies. A. Fluorescent images of initial Q neuroblasts morphologies, when polarization is just beginning in control and *catp-8(gk860114)* mutant animals, imaged 1.5 hours after hatching. Left and right sides of the animals are shown as indicated. Scale bar = 5 μm. B.—C. Quantification of DMA-1::GFP puncta either in the primary (B) or on the tertiary (C) dendrite 100μm anterior of the cell body in the genotypes indicated. ns, not significant, Mann-Whitney test. n = 14 animals per genotype. D. Number of HPO-30::tagBFP puncta in the primary dendrite 100 μm anterior to the cell body in control or *catp-8* mutant animals, presented as mean ± 95% confidence interval. ns not significant, Mann-Whitney test. n = 10 animals per genotype. E. Fluorescent images of animals expressing a functional fosmid based SAX-7::GFP reporter (*ddIs290*) in control, *catp-8(gk860114)* mutants, and animals overexpressing *catp-8* in the epidermis *(dzSi3)*. White arrowheads denote neuronal staining, while open arrows indicate examples of epidermal staining at the lateral epidermal ridge. F. Quantification of the percentage of animals with PVD 4° branching defects in the indicated genotypes in a *ddIs290* background. Statistical comparisons were performed using the Z-test. ****, $P < 0.0005$, ns not significant. n = 15 animals per genotype. G. Fluorescent images of animals expressing *lect-2*::*mNG* endogenous knock-in (*dz249*) [38] in control and *catp-8(gk860114)* mutant animals. White arrowheads denote neuronal staining, while open arrows indicate examples of epidermal staining at the lateral epidermal ridge.
(TIFF)

Acknowledgments

We thank S. Emmons, A. Meléndez, Y. Salzberg, and members of the Bülow laboratory for comments on the manuscript and for helpful discussions during the course of this project. We thank S. Cook for the initial observation of PQR cell migration defects, R. Poole for help with

the analysis of whole genome sequencing data and, Yuji Kohara for cDNA clones and M. Harterink for a plasmid; some strains were provided by the CGC, which is funded by NIH Office of Research Infrastructure Programs.

Author Contributions

Conceptualization: Leo T. H. Tang, Meera Trivedi, Jenna Freund, Barth D. Grant, Hannes E. Bülow.

Data curation: Leo T. H. Tang, Meera Trivedi, Jenna Freund, Christopher J. Salazar, Nelson J. Ramirez-Suarez, Hannes E. Bülow.

Formal analysis: Leo T. H. Tang, Meera Trivedi, Jenna Freund, Christopher J. Salazar, Maisha Rahman, Garrett Lee, Yu Wang, Hannes E. Bülow.

Funding acquisition: Barth D. Grant, Hannes E. Bülow.

Investigation: Leo T. H. Tang, Meera Trivedi, Jenna Freund, Christopher J. Salazar, Maisha Rahman, Nelson J. Ramirez-Suarez, Garrett Lee, Yu Wang.

Project administration: Hannes E. Bülow.

Resources: Barth D. Grant, Hannes E. Bülow.

Supervision: Barth D. Grant, Hannes E. Bülow.

Visualization: Leo T. H. Tang, Meera Trivedi, Christopher J. Salazar, Maisha Rahman, Hannes E. Bülow.

Writing – original draft: Hannes E. Bülow.

Writing – review & editing: Leo T. H. Tang, Meera Trivedi, Jenna Freund, Nelson J. Ramirez-Suarez, Hannes E. Bülow.

References

1. Marin O, Valiente M, Ge X, Tsai LH. Guiding neuronal cell migrations. Cold Spring Harbor perspectives in biology. 2010; 2(2):a001834. https://doi.org/10.1101/cshperspect.a001834 PMID: 20182622; PubMed Central PMCID: PMC2828271.
2. Francis F, Cappello S. Neuronal migration and disorders—an update. Curr Opin Neurobiol. 2020; 66:57–68. Epub 2020/10/24. https://doi.org/10.1016/j.conb.2020.10.002 PMID: 33096394.
3. Dickson BJ. Molecular mechanisms of axon guidance. Science. 2002; 298(5600):1959–64. https://doi.org/10.1126/science.1072165 PMID: 12471249.
4. Sanes JR, Zipursky SL. Synaptic Specificity, Recognition Molecules, and Assembly of Neural Circuits. Cell. 2020; 181(6):1434–5. Epub 2020/06/13. https://doi.org/10.1016/j.cell.2020.05.046 PMID: 32531247.
5. Dong X, Shen K, Bülow HE. Intrinsic and extrinsic mechanisms of dendritic morphogenesis. Annu Rev Physiol. 2015; 77:271–300. https://doi.org/10.1146/annurev-physiol-021014-071746 PMID: 25386991.
6. Jan YN, Jan LY. Branching out: mechanisms of dendritic arborization. Nat Rev Neurosci. 2010; 11 (5):316–28. Epub 2010/04/21. nrn2836 [pii] https://doi.org/10.1038/nrn2836 PMID: 20404840.
7. Lefebvre JL. Molecular mechanisms that mediate dendrite morphogenesis. Current Topics in Developmental Biology: Academic Press; 2021.
8. Inberg S, Meledin A, Kravtsov V, Iosilevskii Y, Oren-Suissa M, Podbilewicz B. Lessons from Worm Dendritic Patterning. Annu Rev Neurosci. 2019; 42:365–83. Epub 2019/04/03. https://doi.org/10.1146/annurev-neuro-072116-031437 PMID: 30939099.
9. Sundararajan L, Stern J, Miller DM, 3rd. Mechanisms that regulate morphogenesis of a highly branched neuron in C. elegans. Dev Biol. 2019; 451(1):53–67. Epub 2019/04/21. https://doi.org/10.1016/j.ydbio.2019.04.002 PMID: 31004567.

10. Desai C, Garriga G, McIntire SL, Horvitz HR. A genetic pathway for the development of the Caenorhabditis elegans HSN motor neurons. Nature. 1988; 336(6200):638–46. https://doi.org/10.1038/336638a0 PMID: 3200316

11. Middelkoop TC, Korswagen HC. Development and migration of the C. elegans Q neuroblasts and their descendants. WormBook. 2014:1–23. Epub 2014/10/16. https://doi.org/10.1895/wormbook.1.173.1 PMID: 25317540; PubMed Central PMCID: PMC4781233.

12. Wadsworth WG, Hedgecock EM. Guidance of neuroblast migrations and axonal projections in Caenorhabditis elegans. Curr Opin Neurobiol. 1992; 2(1):36–41. https://doi.org/10.1016/0959-4388(92)90159-i PMID: 1638133

13. Zinovyeva AY, Yamamoto Y, Sawa H, Forrester WC. Complex network of Wnt signaling regulates neuronal migrations during Caenorhabditis elegans development. Genetics. 2008; 179(3):1357–71. https://doi.org/10.1534/genetics.108.090290 PMID: 18622031; PubMed Central PMCID: PMC2475739.

14. Palmgren MG, Axelsen KB. Evolution of P-type ATPases. Biochim Biophys Acta. 1998; 1365(1–2):37–45. Epub 1998/08/07. https://doi.org/10.1016/s0005-2728(98)00041-3 PMID: 9693719.

15. Palmgren MG, Nissen P. P-type ATPases. Annu Rev Biophys. 2011; 40:243–66. Epub 2011/03/01. https://doi.org/10.1146/annurev.biophys.093008.131331 PMID: 21351879.

16. Sørensen DM, Buch-Pedersen MJ, Palmgren MG. Structural divergence between the two subgroups of P5 ATPases. Biochim Biophys Acta. 2010; 1797(6–7):846–55. Epub 2010/04/27. https://doi.org/10.1016/j.bbabio.2010.04.010 PMID: 20416272.

17. van Veen S, Martin S, Van den Haute C, Benoy V, Lyons J, Vanhoutte R, et al. ATP13A2 deficiency disrupts lysosomal polyamine export. Nature. 2020; 578(7795):419–24. Epub 2020/01/31. https://doi.org/10.1038/s41586-020-1968-7 PMID: 31996848.

18. Ticconi CA, Delatorre CA, Lahner B, Salt DE, Abel S. Arabidopsis pdr2 reveals a phosphate-sensitive checkpoint in root development. Plant J. 2004; 37(6):801–14. Epub 2004/03/05. https://doi.org/10.1111/j.1365-313x.2004.02005.x PMID: 14996215.

19. Ticconi CA, Lucero RD, Sakhonwasee S, Adamson AW, Creff A, Nussaume L, et al. ER-resident proteins PDR2 and LPR1 mediate the developmental response of root meristems to phosphate availability. Proc Natl Acad Sci U S A. 2009; 106(33):14174–9. Epub 2009/08/12. https://doi.org/10.1073/pnas.0901778106 PMID: 19666499; PubMed Central PMCID: PMC2723163.

20. Jakobsen MK, Poulsen LR, Schulz A, Fleurat-Lessard P, Moller A, Husted S, et al. Pollen development and fertilization in Arabidopsis is dependent on the MALE GAMETOGENESIS IMPAIRED ANTHERS gene encoding a type V P-type ATPase. Genes Dev. 2005; 19(22):2757–69. Epub 2005/11/18. https://doi.org/10.1101/gad.357305 PMID: 16291648; PubMed Central PMCID: PMC1283967.

21. Sørensen DM, Holen HW, Pedersen JT, Martens HJ, Silvestro D, Stanchev LD, et al. The P5A ATPase Spf1p is stimulated by phosphatidylinositol 4-phosphate and influences cellular sterol homeostasis. Mol Biol Cell. 2019; 30(9):1069–84. Epub 2019/02/21. https://doi.org/10.1091/mbc.E18-06-0365 PMID: 30785834; PubMed Central PMCID: PMC6724510.

22. Krumpe K, Frumkin I, Herzig Y, Rimon N, Ozbalci C, Brugger B, et al. Ergosterol content specifies targeting of tail-anchored proteins to mitochondrial outer membranes. Mol Biol Cell. 2012; 23(20):3927–35. Epub 2012/08/25. https://doi.org/10.1091/mbc.E11-12-0994 PMID: 22918956; PubMed Central PMCID: PMC3469509.

23. Feng Z, Zhao Y, Li T, Nie W, Yang X, Wang X, et al. CATP-8/P5A ATPase Regulates ER Processing of the DMA-1 Receptor for Dendritic Branching. Cell Rep. 2020; 32(10):108101. Epub 2020/09/10. https://doi.org/10.1016/j.celrep.2020.108101 PMID: 32905774.

24. Qin Q, Zhao T, Zou W, Shen K, Wang X. An Endoplasmic Reticulum ATPase Safeguards Endoplasmic Reticulum Identity by Removing Ectopically Localized Mitochondrial Proteins. Cell Rep. 2020; 33(6):108363. Epub 2020/11/12. https://doi.org/10.1016/j.celrep.2020.108363 PMID: 33176140.

25. McKenna MJ, Sim SI, Ordureau A, Wei L, Harper JW, Shao S, et al. The endoplasmic reticulum P5A-ATPase is a transmembrane helix dislocase. Science. 2020; 369(6511). Epub 2020/09/26. https://doi.org/10.1126/science.abc5809 PMID: 32973005.

26. Minevich G, Park DS, Blankenberg D, Poole RJ, Hobert O. CloudMap: a cloud-based pipeline for analysis of mutant genome sequences. Genetics. 2012; 192(4):1249–69. https://doi.org/10.1534/genetics.112.144204 PMID: 23051646; PubMed Central PMCID: PMC3512137.

27. Albeg A, Smith CJ, Chatzigeorgiou M, Feitelson DG, Hall DH, Schafer WR, et al. C. elegans multi-dendritic sensory neurons: morphology and function. Mol Cell Neurosci. 2011; 46(1):308–17. Epub 2010/10/26. S1044-7431(10)00246-0 [pii] https://doi.org/10.1016/j.mcn.2010.10.001 PMID: 20971193.

28. Smith CJ, Watson JD, Spencer WC, O'Brien T, Cha B, Albeg A, et al. Time-lapse imaging and cell-specific expression profiling reveal dynamic branching and molecular determinants of a multi-dendritic nociceptor in C. elegans. Dev Biol. 2010; 345(1):18–33. Epub 2010/06/12. S0012-1606(10)00805-5 [pii] https://doi.org/10.1016/j.ydbio.2010.05.502 PMID: 20537990.

29. Oren-Suissa M, Hall DH, Treinin M, Shemer G, Podbilewicz B. The fusogen EFF-1 controls sculpting of mechanosensory dendrites. Science. 2010; 328(5983):1285–8. https://doi.org/10.1126/science.1189095 PMID: 20448153; PubMed Central PMCID: PMC3057141.

30. Salzberg Y, Diaz-Balzac CA, Ramirez-Suarez NJ, Attreed M, Tecle E, Desbois M, et al. Skin-Derived Cues Control Arborization of Sensory Dendrites in Caenorhabditis elegans. Cell. 2013; 155(2):308–20. https://doi.org/10.1016/j.cell.2013.08.058 PMID: 24120132.

31. Thompson O, Edgley M, Strasbourger P, Flibotte S, Ewing B, Adair R, et al. The million mutation project: a new approach to genetics in Caenorhabditis elegans. Genome Res. 2013; 23(10):1749–62. https://doi.org/10.1101/gr.157651.113 PMID: 23800452; PubMed Central PMCID: PMC3787271.

32. Anazi S, Maddirevula S, Salpietro V, Asi YT, Alsahli S, Alhashem A, et al. Expanding the genetic heterogeneity of intellectual disability. Hum Genet. 2017; 136(11–12):1419–29. Epub 2017/09/25. https://doi.org/10.1007/s00439-017-1843-2 PMID: 28940097.

33. Sulston JE, Schierenberg E, White JG, Thomson JN. The embryonic cell lineage of the nematode Caenorhabditis elegans. Dev Biol. 1983; 100(1):64–119. https://doi.org/10.1016/0012-1606(83)90201-4 PMID: 6684600

34. Sulston JE, Horvitz HR. Post-embryonic cell lineages of the nematode, Caenorhabditis elegans. Dev Biol. 1977; 56(1):110–56. https://doi.org/10.1016/0012-1606(77)90158-0 PMID: 838129

35. Cronin SR, Rao R, Hampton RY. Cod1p/Spf1p is a P-type ATPase involved in ER function and Ca2+ homeostasis. J Cell Biol. 2002; 157(6):1017–28. Epub 2002/06/12. https://doi.org/10.1083/jcb.200203052 PMID: 12058017; PubMed Central PMCID: PMC2174042.

36. Gilleard JS, Barry JD, Johnstone IL. cis regulatory requirements for hypodermal cell-specific expression of the Caenorhabditis elegans cuticle collagen gene dpy-7. Mol Cell Biol. 1997; 17(4):2301–11. https://doi.org/10.1128/MCB.17.4.2301 PMID: 9121480.

37. Sundararajan L, Smith CJ, Watson JD, Millis BA, Tyska MJ, Miller DM 3rd. Actin assembly and non-muscle myosin activity drive dendrite retraction in an UNC-6/Netrin dependent self-avoidance response. PLoS Genet. 2019; 15(6):e1008228. Epub 2019/06/21. https://doi.org/10.1371/journal.pgen.1008228 PMID: 31220078; PubMed Central PMCID: PMC6605669.

38. Diaz-Balzac CA, Rahman M, Lazaro-Pena MI, Martin Hernandez LA, Salzberg Y, Aguirre-Chen C, et al. Muscle- and Skin-Derived Cues Jointly Orchestrate Patterning of Somatosensory Dendrites. Curr Biol. 2016; 26(17):2379–87. https://doi.org/10.1016/j.cub.2016.07.008 PMID: 27451901; PubMed Central PMCID: PMC5021591.

39. Zou W, Shen A, Dong X, Tugizova M, Xiang YK, Shen K. A multi-protein receptor-ligand complex underlies combinatorial dendrite guidance choices in C. elegans. Elife. 2016; 5. https://doi.org/10.7554/eLife.18345 PMID: 27705746; PubMed Central PMCID: PMC5079751.

40. Tang LT, Diaz-Balzac CA, Rahman M, Ramirez-Suarez NJ, Salzberg Y, Lazaro-Pena MI, et al. TIAM-1/GEF can shape somatosensory dendrites independently of its GEF activity by regulating F-actin localization. Elife. 2019; 8. https://doi.org/10.7554/eLife.38949 PMID: 30694177; PubMed Central PMCID: PMC6370339.

41. Taylor CA, Yan J, Howell AS, Dong X, Shen K. RAB-10 Regulates Dendritic Branching by Balancing Dendritic Transport. PLoS Genet. 2015; 11(12):e1005695. https://doi.org/10.1371/journal.pgen.1005695 PMID: 26633194; PubMed Central PMCID: PMC4669152.

42. Zou W, Yadav S, DeVault L, Nung Jan Y, Sherwood DR. RAB-10-Dependent Membrane Transport Is Required for Dendrite Arborization. PLoS Genet. 2015; 11(9):e1005484. https://doi.org/10.1371/journal.pgen.1005484 PMID: 26394140; PubMed Central PMCID: PMC4578882.

43. Whangbo J, Kenyon C. A Wnt signaling system that specifies two patterns of cell migration in C. elegans. Mol Cell. 1999; 4(5):851–8. https://doi.org/10.1016/s1097-2765(00)80394-9 PMID: 10619031

44. Harterink M, Kim DH, Middelkoop TC, Doan TD, van Oudenaarden A, Korswagen HC. Neuroblast migration along the anteroposterior axis of C. elegans is controlled by opposing gradients of Wnts and a secreted Frizzled-related protein. Development. 2011; 138(14):2915–24. https://doi.org/10.1242/dev.064733 PMID: 21653614; PubMed Central PMCID: PMC3119304.

45. Pani AM, Goldstein B. Direct visualization of a native Wnt in vivo reveals that a long-range Wnt gradient forms by extracellular dispersal. Elife. 2018; 7. https://doi.org/10.7554/eLife.38325 PMID: 30106379; PubMed Central PMCID: PMC6143344.

46. Garriga G, Desai C, Horvitz HR. Cell interactions control the direction of outgrowth, branching and fasciculation of the HSN axons of Caenorhabditis elegans. Development. 1993; 117(3):1071–87. PMID: 8325236

47. Saied-Santiago K, Townley RA, Attonito JD, da Cunha DS, Diaz-Balzac CA, Tecle E, et al. Coordination of Heparan Sulfate Proteoglycans with Wnt Signaling To Control Cellular Migrations and Positioning in Caenorhabditis elegans. Genetics. 2017. https://doi.org/10.1534/genetics.116.198739 PMID: 28576860.

48. Honigberg L, Kenyon C. Establishment of left/right asymmetry in neuroblast migration by UNC- 40/DCC, UNC-73/Trio and DPY-19 proteins in C. elegans. Development. 2000; 127(21):4655–68. PMID: 11023868

49. Buettner FF, Ashikov A, Tiemann B, Lehle L, Bakker H. C. elegans DPY-19 is a C-mannosyltransferase glycosylating thrombospondin repeats. Mol Cell. 2013; 50(2):295–302. Epub 2013/04/09. https://doi.org/10.1016/j.molcel.2013.03.003 PMID: 23562325.

50. Middelkoop TC, Williams L, Yang PT, Luchtenberg J, Betist MC, Ji N, et al. The thrombospondin repeat containing protein MIG-21 controls a left-right asymmetric Wnt signaling response in migrating C. elegans neuroblasts. Dev Biol. 2012; 361(2):338–48. Epub 2011/11/15. https://doi.org/10.1016/j.ydbio.2011.10.029 PMID: 22074987.

51. Schmitz C, Wacker I, Hutter H. The Fat-like cadherin CDH-4 controls axon fasciculation, cell migration and hypodermis and pharynx development in Caenorhabditis elegans. Dev Biol. 2008; 316(2):249–59. Epub 2008/03/11. https://doi.org/10.1016/j.ydbio.2008.01.024 PMID: 18328472.

52. Sundararajan L, Norris ML, Schoneich S, Ackley BD, Lundquist EA. The fat-like cadherin CDH-4 acts cell-non-autonomously in anterior-posterior neuroblast migration. Dev Biol. 2014; 392(2):141–52. Epub 2014/06/24. https://doi.org/10.1016/j.ydbio.2014.06.009 PMID: 24954154; PubMed Central PMCID: PMC4136450.

53. Ebbing A, Middelkoop TC, Betist MC, Bodewes E, Korswagen HC. Partially overlapping guidance pathways focus the activity of UNC-40/DCC along the anteroposterior axis of polarizing neuroblasts. Development. 2019; 146(18). Epub 2019/09/07. https://doi.org/10.1242/dev.180059 PMID: 31488562.

54. Salser SJ, Kenyon C. Activation of a C. elegans Antennapedia homologue in migrating cells controls their direction of migration. Nature. 1992; 355(6357):255–8. https://doi.org/10.1038/355255a0 PMID: 1346230.

55. Wadsworth WG, Bhatt H, Hedgecock EM. Neuroglia and pioneer neurons express UNC-6 to provide global and local netrin cues for guiding migrations in C. elegans. Neuron. 1996; 16(1):35–46. https://doi.org/10.1016/s0896-6273(00)80021-5 PMID: 8562088

56. Zallen JA, Yi BA, Bargmann CI. The conserved immunoglobulin superfamily member SAX-3/Robo directs multiple aspects of axon guidance in C. elegans. Cell. 1998; 92(2):217–27. https://doi.org/10.1016/s0092-8674(00)80916-2 PMID: 9458046

57. Chien J, Devkota R, Yosef N, Mörck C. Regulation of Axon Guidance by the Wnt Receptor Ror/CAM-1 in the PVT Guidepost Cell in Caenorhabditis elegans. Genetics. 2017; 207(4):1533–45. Epub 2017/10/11. https://doi.org/10.1534/genetics.117.300375 PMID: 28993416; PubMed Central PMCID: PMC5714464.

58. Salzberg Y, Ramirez-Suarez NJ, Bülow HE. The proprotein convertase KPC-1/furin controls branching and self-avoidance of sensory dendrites in Caenorhabditis elegans. PLoS Genet. 2014; 10(9):e1004657. https://doi.org/10.1371/journal.pgen.1004657 PMID: 25232734; PubMed Central PMCID: PMC4169376.

59. Dong X, Chiu H, Park YJ, Zou W, Zou Y, Ozkan E, et al. Precise regulation of the guidance receptor DMA-1 by KPC-1/Furin instructs dendritic branching decisions. Elife. 2016; 5. https://doi.org/10.7554/eLife.11008 PMID: 26974341; PubMed Central PMCID: PMC4811766.

60. Ochs ME, Josephson MP, Lundquist EA. The Predicted RNA-Binding Protein ETR-1/CELF1 Acts in Muscles To Regulate Neuroblast Migration in Caenorhabditis elegans. G3. 2020; 10(7):2365–76. Epub 2020/05/14. https://doi.org/10.1534/g3.120.401182 PMID: 32398235; PubMed Central PMCID: PMC7341121.

61. Josephson MP, Miltner AM, Lundquist EA. Nonautonomous Roles of MAB-5/Hox and the Secreted Basement Membrane Molecule SPON-1/F-Spondin in Caenorhabditis elegans Neuronal Migration. Genetics. 2016; 203(4):1747–62. Epub 2016/05/27. https://doi.org/10.1534/genetics.116.188367 PMID: 27225683; PubMed Central PMCID: PMC4981275.

62. Smith CJ, O'Brien T, Chatzigeorgiou M, Spencer WC, Feingold-Link E, Husson SJ, et al. Sensory Neuron Fates Are Distinguished by a Transcriptional Switch that Regulates Dendrite Branch Stabilization. Neuron. 2013; 79(2):266–80. https://doi.org/10.1016/j.neuron.2013.05.009 PMID: 23889932.

63. Brenner S. The genetics of Caenorhabditis elegans. Genetics. 1974; 77(1):71–94. PMID: 4366476

64. Nance J, Frokjaer-Jensen C. The Caenorhabditis elegans Transgenic Toolbox. Genetics. 2019; 212(4):959–90. Epub 2019/08/14. https://doi.org/10.1534/genetics.119.301506 PMID: 31405997; PubMed Central PMCID: PMC6707460.

65. Bülow HE, Hobert O. Differential sulfations and epimerization define heparan sulfate specificity in nervous system development. Neuron. 2004; 41(5):723–36. https://doi.org/10.1016/s0896-6273(04)00084-4 PMID: 15003172.

66. Zallen JA, Kirch SA, Bargmann CI. Genes required for axon pathfinding and extension in the C. elegans nerve ring. Development. 1999; 126(16):3679–92. PMID: 10409513

67. Clark SG, Chiu C. C. elegans ZAG-1, a Zn-finger-homeodomain protein, regulates axonal development and neuronal differentiation. Development. 2003; 130(16):3781–94. https://doi.org/10.1242/dev.00571 PMID: 12835394.